Production of deuterons, tritons, 3He nuclei, and their antinuclei in pp collisions at √s = 0.9, 2.76, and 7 TeV

(ALICE Collaboration) Acharya, S.; ...; Antičić, Tome; ...; Erhardt, Filip; ...; Gotovac, Sven; ...; Jerčić, Marko; ...; ...

Source / Izvornik: **Physical Review C, 2018, 97**

Journal article, Published version
Rad u časopisu, Objavljena verzija rada (izdavačev PDF)

https://doi.org/10.1103/PhysRevC.97.024615

Permanent link / Trajna poveznica: https://urn.nsk.hr/urn:nbn:hr:217:592896

Production of deuterons, tritons, ^{3}He nuclei, and their antinuclei in pp collisions at $\sqrt{s} = 0.9$, 2.76, and 7 TeV

S. Acharya *et al.*[*]
(ALICE Collaboration)

(Received 23 October 2017; published 21 February 2018)

Invariant differential yields of deuterons and antideuterons in pp collisions at $\sqrt{s} = 0.9$, 2.76 and 7 TeV and the yields of tritons, ^{3}He nuclei, and their antinuclei at $\sqrt{s} = 7$ TeV have been measured with the ALICE detector at the CERN Large Hadron Collider. The measurements cover a wide transverse momentum (p_{T}) range in the rapidity interval $|y| < 0.5$, extending both the energy and the p_{T} reach of previous measurements up to 3 GeV/c for $A = 2$ and 6 GeV/c for $A = 3$. The coalescence parameters of (anti)deuterons and $^3\overline{\mathrm{He}}$ nuclei exhibit an increasing trend with p_{T} and are found to be compatible with measurements in pA collisions at low p_{T} and lower energies. The integrated yields decrease by a factor of about 1000 for each increase of the mass number with one (anti)nucleon. Furthermore, the deuteron-to-proton ratio is reported as a function of the average charged particle multiplicity at different center-of-mass energies.

DOI: 10.1103/PhysRevC.97.024615

I. INTRODUCTION

The production of light nuclei and antinuclei has been measured in many experiments at energies lower than those of the Large Hadron Collider (LHC). Deuterons and antideuterons are copiously produced in heavy-ion collisions [1–11], but less abundantly in lighter particle collisions, such as pp [12,13] and $\overline{p}p$ [14] collisions, photoproduction γp [15], and e^+e^- annihilation at $\Upsilon(nS)$ [16] and Z^0 [17] energies. Measurements of heavier antinuclei, such as antitritons and $^3\overline{\mathrm{He}}$ nuclei, have only been reported in pA [18,19] and AA collisions [11,20–23].

The high luminosity provided by the LHC allows these measurements to be extended to higher energies and transverse momenta (p_{T}) than in previous experiments, and provides in addition the possibility to detect for the first time antinuclei heavier than antideuterons in pp collisions. Many of these measurements have been explained as the result of the coalescence of protons and neutrons that are nearby in space and have similar velocities [24,25], but this has not been experimentally tested in high p_{T} regimes in small systems. On the other hand, statistical hadronization models [11,26] have been successful in describing particle yields over a wide range of energies in AA collisions, with the chemical freeze-out temperature and baryochemical potential being constrained by measurements of particle ratios. In this sense, the deuteron-to-proton ratio could serve as a test for possible thermal-statistical behavior in pp collisions at LHC energies.

On a broader level, this subject may also have an impact on cosmology. Big-bang nucleosynthesis is the dominant natural source of deuterons [27] and, in the absence of baryogenesis, one could assume that the same holds for antideuterons. These antinuclei and even heavier antinuclei can also be produced in pp and pA collisions in interstellar space, representing a background source in the searches for segregated primordial antimatter and dark matter [28–30]. As it turns out, the low momentum characteristic yields of antinuclei at central rapidities (compared to forward) lie in an energy region which is best suited for identification by most satellite-borne (low magnetic-field) instruments, such as AMS-02 [28].

While the differential yields of deuterons in pp collisions at $\sqrt{s} = 7$ TeV have been reported in [11], this paper complements the previously published results by providing the corresponding measurements of antideuterons at the same collision energy. In addition, results for (anti)deuterons at $\sqrt{s} = 0.9$ and 2.76 TeV as well as for (anti)tritons and ^{3}He (anti)nuclei at $\sqrt{s} = 7$ TeV are given. The paper is organized as follows: Section II gives a description of the experimental apparatus. Section III describes the analysis procedure of the experimental data along with the estimation of the systematic uncertainties. In Sec. IV, the distributions of (anti)deuterons, (anti)tritons, and ^{3}He (anti)nuclei are presented. The integrated yields, the deuteron-to-proton ratios, and the coalescence parameters, which relate the production of nuclei with those of the nucleons, are obtained in Sec. V and the summary and conclusions are presented in Sec. VI.

II. EXPERIMENTAL APPARATUS

ALICE [31–33] is a multipurpose detector designed to study heavy-ion collisions at the LHC and it also has excellent capabilities to study light nuclei and antinuclei in pp collisions. The nuclei were identified using the central detectors: the inner tracking system (ITS), the time projection chamber (TPC), and

[*]Full author list given at the end of the article.

the time of flight (TOF) detector. These detectors are located inside a solenoidal magnetic field with a strength of 0.5 T and cover the full azimuthal acceptance and the pseudorapidity range $|\eta| < 0.9$.

The ITS [34] consists of six cylindrical layers of position-sensitive detectors, covering the central rapidity region for vertices located in $|z| < 10$ cm, where z is the distance along the particle beam direction. The two innermost layers are silicon pixel detectors (SPD), followed by two layers of silicon drift detectors (SDD), while the two outermost layers are double-sided silicon strip detectors (SSD). The ITS is mainly used for reconstruction of the primary and secondary vertices. It also helps to separate primary nuclei from secondary nuclei via the determination of the distance of closest approach of the track to the primary vertex. The TPC [35], the main tracking component of ALICE, is a large drift detector with a low material budget to reduce multiple scattering and secondary particle production. In combination with the ITS, it is used to measure particle momenta. The TPC is also used to identify particles via their specific ionization energy loss with a resolution of 5% in pp collisions [36]. The TOF [37] detector is a large-area array of multigap resistive plate chambers covering the full azimuth $0 \leqslant \phi < 2\pi$ and $|\eta| < 0.9$, except the region $260^\circ < \phi < 320^\circ$ and $|\eta| < 0.12$ to avoid covering the photon spectrometer with more material. In pp collisions, it measures the time of flight of particles with an overall resolution of about 120 ps, allowing the identification of light nuclei and antinuclei with transverse momenta above 3 GeV/c, depending on the available data. The start time for the time of flight is provided by the T0 detector, with a time resolution of ∼40 ps. The T0 consists of two arrays of Cherenkov counters, T0A and T0C, placed on opposite sides of the interaction point at $z = 375.0$ cm and $z = -72.7$ cm, respectively. If there is no T0 signal, the TOF detector is used to measure the start time when at least three particles reach the TOF detector [38].

Between the TPC and TOF detector there is a transition radiation detector (TRD) [33] to discriminate between electrons and pions above 1 GeV/c. Only 7 modules out of 18 were installed for the pp run of 2010, leaving the major part of space between TPC and TOF free of additional material. The V0 detector [39], two hodoscopes of 32 scintillator cells each which cover the pseudorapidity ranges $2.8 < \eta < 5.1$ and $-3.7 < \eta < -1.7$, provides in combination with the SPD the trigger for inelastic pp collisions.

III. DATA ANALYSIS

The pp events used in this paper were collected by the ALICE Collaboration during 2010 and 2011. The recorded integrated luminosity for each analyzed sample is 0.124 nb^{-1}, 0.692 nb^{-1}, and 4.20 nb^{-1} for the center-of-mass energies $\sqrt{s} = 0.9$, 2.76, and 7 TeV, respectively.

A. Event and track selection

The pp events were triggered by requiring a hit in both sides of the V0, i.e., two charged particles separated by approximately 4.5 units of pseudorapidity, which suppresses single diffractive events. The presence of passing bunches was detected by two beam-pickup counters. Contamination from beam-induced background was rejected offline using the timing information of the V0. Additionally, a cut on the correlation between the number of SPD clusters and the number of small track segments (tracklets) in the SPD detector was applied. Furthermore, in order to maintain a uniform acceptance and to reduce beam-induced noise, collision vertices were required to be within 10 cm of the center of the detector in the beam direction and within 1 cm in the transverse direction. Pile-up events were reduced by requiring that more than three tracklets or tracks contribute to the reconstructed vertex. In cases of multiple vertices which are separated by more than 0.8 cm, the vertex reconstruction with the SPD allows these events to be tagged as pile-up and hence not considered in the analysis. The events analyzed here consist mostly of nonsingle diffractive events, which represent a fraction of the total inelastic cross section equal to $0.763^{+0.022}_{-0.008}$, $0.760^{+0.052}_{-0.028}$, and $0.742^{+0.050}_{-0.020}$ for $\sqrt{s} = 0.9$, 2.76, and 7 TeV [40], respectively. Those fractions were used to extrapolate the measurements to inelastic pp collisions assuming that the production of nuclei in single diffractive events is not significant with respect to nonsingle diffractive events based on Monte Carlo estimates (less than 3%).

For each track at least two track points were required in the ITS and 70 out of a maximum of 159 in the TPC. A pseudorapidity cut of $|\eta| < 0.8$ was also required to avoid edge effects. Tracks with kinks, typically originating from weak decays inside the TPC volume, were treated as two separate tracks and only the track pointing to the primary vertex was kept.

The measurements are reported for the rapidity interval $|y| < 0.5$ and have been corrected for detector efficiency based on the GEANT3 particle propagation code [41]. Track matching between the TPC and TOF detectors in GEANT3 was further improved by a data driven method based on a study of tracks not crossing the TRD material, resulting in a 6% difference. Since at low p_T many nuclei in $|y| < 0.5$ are outside $|\eta| < 0.8$, their number was extrapolated using a Monte Carlo simulation where the rapidity distribution was approximated by a flat distribution.

In order to allow for a consistent comparison of the antideuteron-to-deuteron ratio across different center-of-mass energies with an identical GEANT version, a reanalysis of the deuteron differential yield at $\sqrt{s} = 7$ TeV is presented here. The results are found to be consistent with the previous measurements shown in [11] within the systematic uncertainties.

B. (Anti)nuclei identification

The identification of nuclei and antinuclei is based on their specific energy loss in the TPC and the estimation of their mass with the TOF detector. Figure 1 shows the energy loss signal recorded by the TPC of different nucleus species versus the rigidity ($p_{TPC}/|Z|$), where p_{TPC} is the momentum estimated at the inner wall of the TPC.

Deuterons and antideuterons can be identified cleanly up to $p_{TPC} \simeq 1.2$ GeV/c, which corresponds to a maximum p_T of 1 GeV/c. For $p_T > 1$ GeV/c a coincidence with a TOF signal was required, in addition to a $\pm 3\sigma$ cut around their expected energy loss in the TPC, extending the identification up

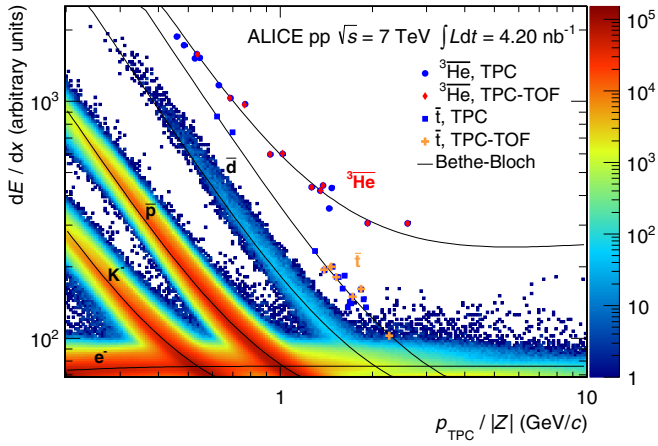

FIG. 1. Energy loss in the TPC (dE/dx) of particles with negative charge versus the rigidity estimated at the TPC inner wall ($p_{\text{TPC}}/|Z|$). The solid lines represent the expected energy loss according to the parametrization of the Bethe-Bloch formula. The blue circles and squares are $^3\overline{\text{He}}$ nuclei and antitritons identified by the TPC only, and the orange crosses and the red diamonds are the antitritons and $^3\overline{\text{He}}$ nuclei, respectively, that were matched to a TOF detector hit.

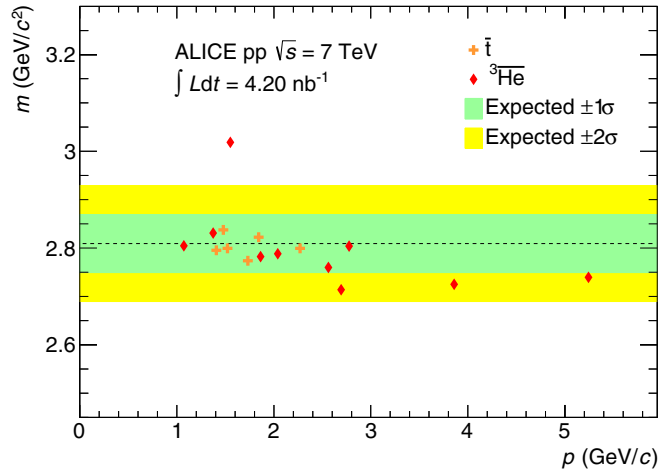

FIG. 3. Mass distribution of antitriton (crosses) and $^3\overline{\text{He}}$ nucleus (diamonds) candidates obtained with the TOF detector as a function of the total momentum. The green and yellow bands represent 1σ and 2σ intervals, respectively, around the expected ^{3}He mass (dashed line), obtained from the TOF resolution.

to $p_{\text{T}} = 3$ GeV/c. For this, tracks were propagated to the outer radius of the TOF detector and, if a hit was found close enough to the trajectory, the corresponding time of flight was assigned to the track. Then, the squared mass $m^2 = p^2(t^2/l^2 - 1)$ was calculated, where p is the reconstructed momentum, t the time of flight, and l the track length. Figure 2 shows the squared mass distribution for several p_{T} bins in the region of the antideuteron squared mass. The antideuteron signal is approximately Gaussian, centered at the deuteron squared mass and with an exponential tail on the high mass side. This exponential tail is also present in the signal of other particle species such as π, K, and p and extends to the antideuteron squared mass, producing an exponential background. The signal was extracted by combining a Gaussian with an exponential tail and an exponential background (Fig. 2).

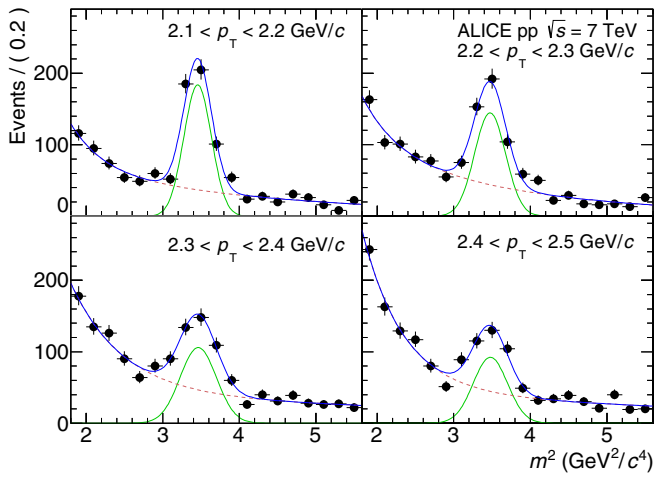

FIG. 2. Squared mass distribution for tracks within $\pm 3\sigma$ of the expected energy loss for antideuterons in the TPC in several p_{T} bins. The solid blue line is the global fit, the dashed line the background, and the green line the antideuteron signal.

Tritons and antitritons were identified by selecting tracks within $\pm 3\sigma$ of their expected energy loss in the TPC and by also requiring a match to a TOF detector hit. The minimum $p_{\text{T}} = 1.2$ GeV/c was chosen to be the same as for the ^{3}He nuclei. Due to the small number of tritons, it was not possible to use the signal extraction procedure used for deuterons. In this case, the selected tracks were required to have an associated mass within $\pm 3\sigma$ ($\sigma \simeq 0.05$ GeV/c^2) of the triton mass and the maximum p_{T} was limited to 1.8 GeV/c. The result is shown in Figs. 1 and 3, with six antitriton candidates in the interval $1.2 < p_{\text{T}} < 1.8$ GeV/c.

Unlike deuterons and tritons, ^{3}He and $^3\overline{\text{He}}$ nuclei can be identified throughout the p_{T} range with the TPC, since for nuclei with $|Z| = 2$ the energy deposition is well separated from particles with $|Z| = 1$. In total, 17 candidates for $^3\overline{\text{He}}$ nuclei were observed, based on the specific energy loss in the TPC (Fig. 1), out of which 14 candidates were in the interval $1.2 < p_{\text{T}} < 6$ GeV/c, and these were used in the measurements. Their identities were confirmed for those particles that were matched to a TOF hit (10 out of 14) with a mass measurement based on their times of flight, as shown in Fig. 3. A few $^3\overline{\text{He}}$ nuclei (six candidates) were also observed at the center-of-mass energy 2.76 TeV.

C. Secondary (anti)nuclei

Secondary nuclei are copiously produced in spallation reactions induced in the detector material by the impact of primary particles. They are also produced in the decays of Λ hypernuclei, with the π-mesonic decay of the (anti)hypertriton being the most important contribution [42].

The distances of closest approach (DCA) of the track to the primary vertex in the transverse plane (DCA_{xy}) and along the beam direction (DCA_z) were used to distinguish and reduce

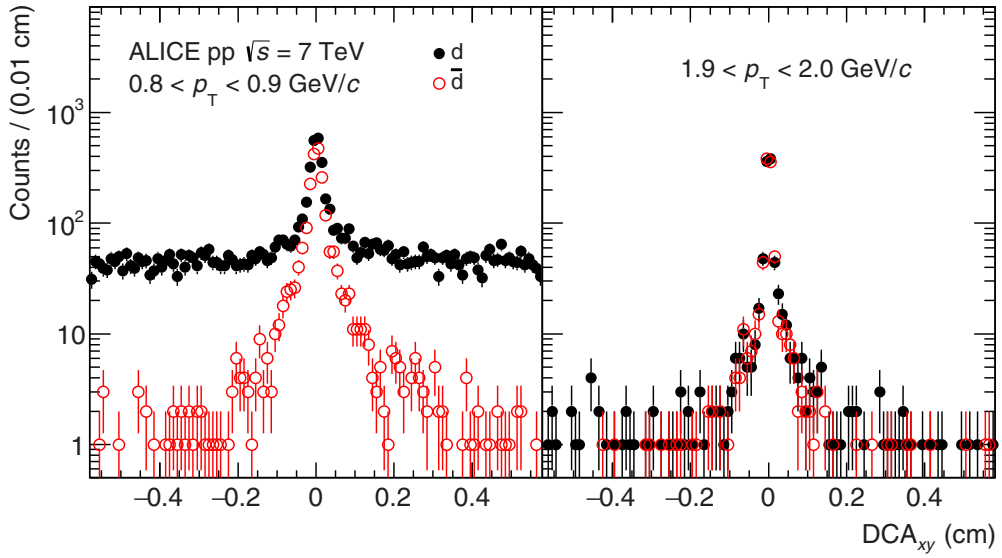

FIG. 4. Distance of closest approach in the transverse plane to the primary vertex (DCA$_{xy}$) of deuterons (solid circles) and antideuterons (hollow circles) for the p_T bins $0.8 < p_T < 0.9$ GeV/c (left) and $1.9 < p_T < 2.0$ GeV/c (right). A large background distribution of secondary deuterons is clearly visible in the left panel.

the number of secondary nuclei. Since they are produced far away from the primary vertex, they have a broader and flatter DCA$_{xy}$ distribution than primary nuclei, which have a narrow DCA$_{xy}$ distribution peaked at zero, similar to antinuclei. Figure 4 illustrates the different DCA$_{xy}$ distributions for deuterons and antideuterons at low and high p_T. A positive DCA$_{xy}$ was assigned when the primary vertex was inside the radius of curvature of the track and a negative value in the opposite case. The number of secondary nuclei was greatly reduced by requiring $|\text{DCA}_{xy}| < 0.2$ cm and $|\text{DCA}_z| < 3$ cm, corresponding to a cut of $\pm 10\sigma$ in the measured DCA resolution in the lowest p_T bin.

The fraction of secondary nuclei with respect to primary nuclei was estimated with DCA$_{xy}$ templates from Monte Carlo simulations for each p_T bin. The templates were fitted to the measured distribution with a maximum likelihood procedure which relies on a Poisson distribution and takes into account both the measured distribution and Monte Carlo statistical uncertainties [43]. This fraction was found to fall exponentially as a function of p_T and was subtracted from the measurements.

The production of antinuclei from interactions of primary particles with the detector material was neglected, since antinuclei exhibit a narrow DCA$_{xy}$ distribution peaked at zero (Fig. 4). Due to the small production cross section of (anti)hypernuclei in pp collisions, the feed-down contribution of (anti)nuclei was not subtracted, but instead included as a systematic uncertainty.

D. Systematic uncertainties

Table I summarizes the values of the systematic uncertainties for the lowest and highest p_T bins. These uncertainties take into account the identification procedure, the track selection criteria, secondary nuclei originating in the detector material and from feed-down, the (anti)nucleus–nucleus interactions simulated in GEANT, and the material budget.

The identification procedure was affected by an uncertainty coming from the background and signal shapes at high p_T, where the signal-to-background ratio was small. It was evaluated by changing the squared mass interval and extracting the signal with two different methods: one by using the procedure described in Sec. III B and the other by counting the number of entries in the $1 < p_T < 1.4$ GeV/c interval where the identification is unambiguous. For antitritons and $^3\overline{\text{He}}$ nuclei the identification was clean and the particle identification uncertainty was assumed to be negligible. Systematic

TABLE I. Summary of the main sources of systematic uncertainties for the lowest and highest p_T bins. Symmetric uncertainties are listed without sign for clarity.

	d	$\bar{d}$	t	$\bar{t}$	^{3}He	$^3\overline{\text{He}}$
p_T (GeV/c)	0.8–3.0	0.8–3.0	1.2–1.8	1.2–1.8	1.2–3.0	1.2–6.0
Particle identification	negl.–20%	negl.–20%	negl.	negl.	negl.	negl.
Track selection	4%	4%	4%	4%	4%	4%
Secondary nuclei	4%	negl.	18%	negl.	20%–negl.	negl.
Feed-down nuclei	negl.	negl.	–6%	–6%	–10%	–10%
Hadronic interactions	6%	6%	12%	12%	6%	6%
Material budget	3%–negl.	3%–negl.	3%	3%	2%–1%	2%–1%

uncertainties due to the track selection criteria were estimated to be less than 4% for nuclei and antinuclei by changing the conditions for selecting tracks.

The approximations made in the DCA_{xy} templates introduced an uncertainty on the removal of secondary nuclei originating in the detector material. A value of 4% was estimated for deuterons by replacing the simulated DCA_{xy} templates of primary deuterons with the measured DCA_{xy} distribution of antideuterons, which are not affected by contamination from secondary tracks. An uncertainty of ∼20% was estimated following a similar procedure for tritons and ^{3}He nuclei.

The dominant feed-down contribution for (anti)nuclei is the π-mesonic decay of (anti)hypertritons [42]: ${}^3_\Lambda\mathrm{H} \to d + p + \pi^-$, ${}^3_\Lambda\mathrm{H} \to d + n + \pi^0$, ${}^3_\Lambda\mathrm{H} \to t + \pi^0$ and ${}^3_\Lambda\overline{\mathrm{H}} \to {}^3\overline{\mathrm{He}} + \pi^+$. In pp collisions, the ${}^3_\Lambda$H cross section was estimated to be of the same order of magnitude as the ^{3}He nucleus cross section [44]. However, the production cross section of deuterons is about 10^4 times greater than that of ^{3}He nuclei, hence the contamination for (anti)deuterons can be considered negligible. Additionally, the fraction of hypertritons which passes the track selection in the ^{3}He (anti)nucleus channel was estimated with a Monte Carlo simulation and is at most 35%. Assuming a similar value for the (anti)triton channel and branching ratios of 27% and 13% [42], then less than ∼10% and ∼6% contamination is expected for ^{3}He (anti)nuclei and (anti)tritons, respectively.

The (anti)nucleus–nucleus elastic and inelastic scattering uncertainty was evaluated by comparing the GEANT3 simulations with the data for two different experimental configurations: one using the detector portion in which the TRD modules were installed between the TPC and the TOF detector and another in which the TRD was not installed. The ratio between the number of (anti)deuterons counted with the two different detector configurations is related to the number of (anti)deuterons lost due to hadronic interactions. These ratios were compared with a GEANT3 simulation and a 6% uncertainty was estimated for the amount of nuclei lost in such processes. This comparison, however, was not feasible for (anti)tritons due to the limited data, and a 12% uncertainty was assumed. Unlike deuterons and tritons, the measurements of ^{3}He (anti)nuclei presented here only rely on TPC information, hence they are not affected by the TRD material in front of the TOF detector.

Another source of systematic uncertainty is the accuracy in the knowledge of the material budget. This uncertainty was estimated to be +3.4% and −6.2% by comparing the material thickness estimated by analyzing photon conversions in the inner detectors with the material description implemented in the Monte Carlo simulations [45]. To propagate these uncertainties to the results, a Monte Carlo simulation was done in which the material density was varied by ±10% and linearly interpolated to match the uncertainties in the material budget. The result was below 3% at low p_{T} and negligible at high p_{T} for the different (anti)nuclei.

The extrapolation of the measurements to inelastic pp collisions adds additional systematic uncertainties of $^{+2.2}_{-0.8}$%, $^{+5.2}_{-2.8}$% and $^{+5.0}_{-2.0}$% for the center-of-mass energies 0.9, 2.76, and 7 TeV, respectively [40]. However, these uncertainties are not included in the figures as in previous related publications [11,46–48].

IV. RESULTS

A. Deuterons and antideuterons

The invariant differential yields of deuterons and antideuterons were measured in the p_{T} range $0.8 < p_{\mathrm{T}} < 3$ GeV/c (Fig. 5) and extrapolated to inelastic pp collisions

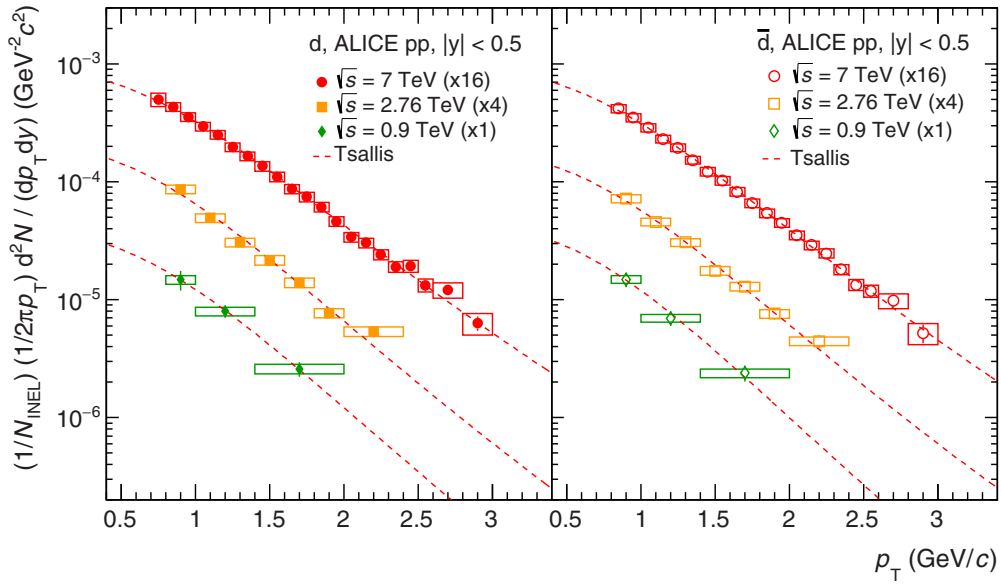

FIG. 5. Invariant differential yield of deuterons (left panel) and antideuterons (right panel) in inelastic pp collisions (INEL) at $\sqrt{s} = 0.9$, 2.76, and 7 TeV. Systematic uncertainties are represented by boxes and the data are multiplied by constant factors for clarity in the figure. The lowest p_{T} point for deuterons at $\sqrt{s} = 7$ TeV was taken from [11]. The dashed line represents the result of a fit with a Tsallis function (see Sec. V B for details).

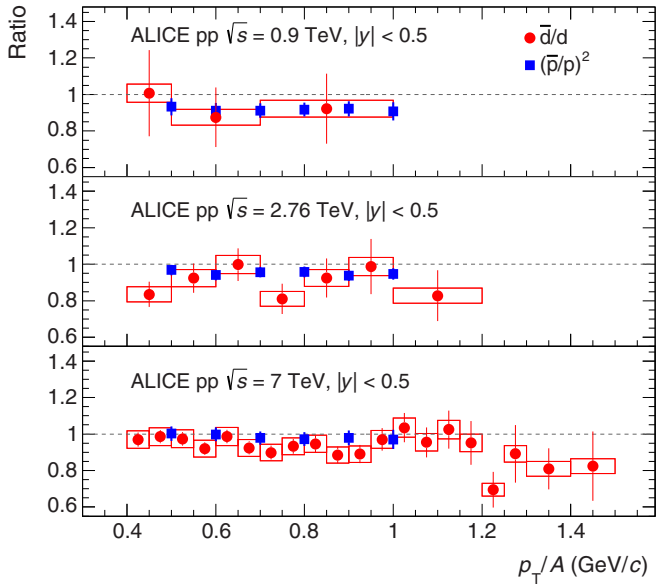

FIG. 6. Antideuteron-to-deuteron ratio ($\bar{d}/d$) as a function of p_T per nucleon in pp collisions compared with the $(\bar{p}/p)^2$ ratio (squares) at mid-rapidity ($|y| < 0.5$) [49,50]. Boxes represent the systematic uncertainties and error bars in the $(\bar{p}/p)^2$ ratios are statistical and systematic uncertainties added in quadrature.

with the cross sections of Ref. [40]. At LHC energies, both nucleus species are produced with similar abundance since the antideuteron-to-deuteron ratio approaches 1 as the center-of-mass energy increases (Fig. 6). The ratios are consistent with the $(\bar{p}/p)^2$ ratios extracted from Refs. [49,50], and hence are in agreement with the expectation from simple coalescence and thermal–statistical models.

B. Heavier nuclei and antinuclei

A recorded luminosity of 4.2 nb^{-1} allowed antitritons and $^3\overline{\mathrm{He}}$ nuclei to be detected in pp collisions. Since the total number of observed candidates is small, the uncertainties were estimated as a central confidence interval (two-sided), using a coverage probability of 68.27% for a Poisson distribution. The resulting invariant yields for both antinucleus species are compatible in the p_T range where measurements were possible (Fig. 7). Some ^{3}He nuclei were also observed in the highest p_T bin, but, since the production rate is very small, it was not feasible to evaluate the contamination due to secondary ^{3}He nuclei, and the bin was then excluded from this measurement. In contrast, $^3\overline{\mathrm{He}}$ nuclei are not affected by this source of contamination, and the three measurements are sufficient to determine the parameters of the Tsallis distribution to extrapolate the yields (see Sec. V B).

V. DISCUSSION

A. Coalescence parameter

Many measurements of light nuclei have been successfully explained as the result of the coalescence of protons and neutrons that are nearby in phase-space [24,25]. In this model, the production of a nucleus with mass number $A = N + Z$ is related to the production of nucleons at equal momentum per nucleon by

$$E_A \frac{d^3N_A}{dp_A^3} = B_A \left(E_p \frac{d^3N_p}{dp_p^3} \right)^Z \left(E_n \frac{d^3N_n}{dp_n^3} \right)^N, \qquad \vec{p}_p = \vec{p}_n = \frac{\vec{p}_A}{A}, \tag{1}$$

where B_A is called the coalescence parameter. This parameter has been found to be constant at low transverse momentum in

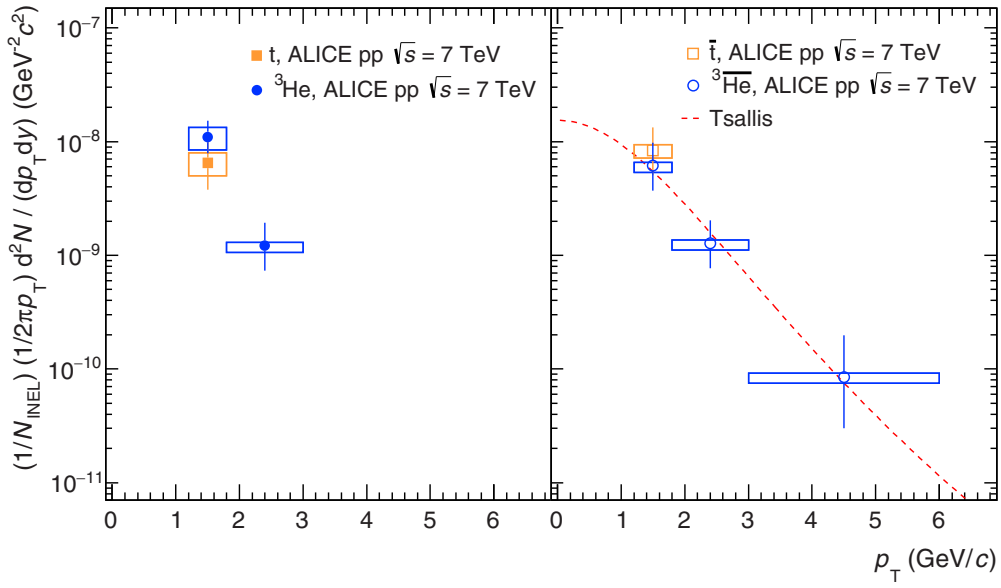

FIG. 7. Invariant differential yields of tritons and ^{3}He nuclei (left panel) and their antinuclei (right panel) in inelastic pp collisions at $\sqrt{s} = 7$ TeV. Error bars and boxes represent the statistical and systematic uncertainties, respectively, and the dashed line the result of a fit with a Tsallis function (see Sec. V B for details).

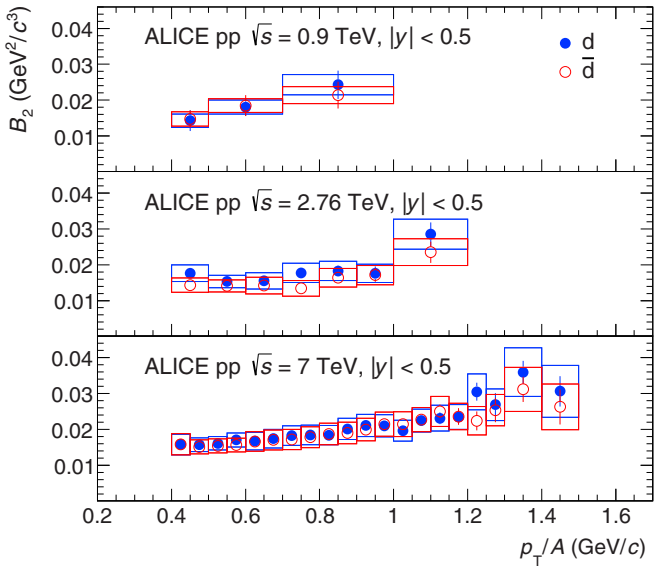

FIG. 8. Coalescence parameter (B_2) of deuterons (solid circles) and antideuterons (hollow circles) as a function of p_T per nucleon in inelastic pp collisions at $\sqrt{s} = 0.9$, 2.76, and 7 TeV. Statistical uncertainties are represented by error bars and systematic uncertainties by boxes.

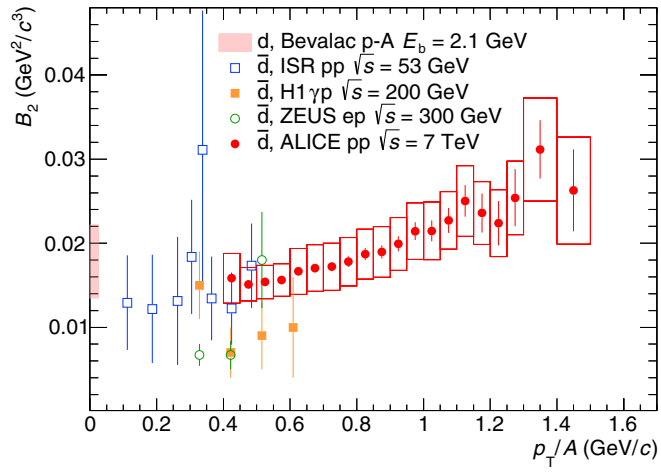

FIG. 9. Coalescence parameter (B_2) of antideuterons in inelastic pp collisions at $\sqrt{s} = 7$ TeV (circles) compared with the values measured at lower energies in pp [12,13], γp [15], ep [51] (squares and hollow circles), and in p-Cu and p-Pb collisions [1] (band at $p_T/A = 0$ GeV/c).

light-particle collisions [15,51]. In contrast, in AA collisions it has been reported that B_A decreases with increasing centrality of the collision, and for each centrality it increases with p_T [8–11].

Assuming equal distribution of nucleons in Eq. (1) and taking the proton and antiproton distributions from Refs. [46–48], the coalescence parameter (B_2) was computed, and it is shown in Fig. 8. The resulting values for deuterons and antideuterons are compatible and do not show any significant dependence on the center-of-mass energy within uncertainties. These measurements extend the p_T reach up to three times beyond previous measurements in pp collisions extracted from the CERN Intersecting Storage Rings (ISR) [12,13,52] (Fig. 9).

To extract the B_2 from the CERN ISR, the antiproton distribution was taken from [52] and the total cross section of 42.3 ± 0.4 mb from [53]. The distribution was also scaled by a factor of 0.69, estimated with an EPOS (LHC) simulation [44,54], to take into account the feed-down contribution. Figure 9 also includes the B_2 parameter of antideuterons from γp collisions and deep inelastic scattering of electrons at the Hadron-Electron Ring Accelerator (HERA) at DESY [15,51] and B_2 from p-Cu and p-Pb collisions at the LBNL Bevalac [1]. Our measurement reveals a p_T dependence in B_2 not seen in previous experiments, which is significant given that the systematic uncertainties are correlated bin by bin.

This p_T dependence can be reproduced with QCD-inspired event generators, such as PYTHIA 8.2 (Monash tune) [55] and EPOS (LHC), when adding a coalescence-based afterburner [44] that takes into account the momentum correlations between nucleons (Fig. 10). The afterburner looks for clusters of nucleons among the final particles produced by the event generators and boosts them to their center-of-mass frame. If the momentum of each individual nucleon is less than a certain value, a nucleus is generated. With the afterburner, a constant B_2 is recovered when selecting protons from one event and neutrons from the next event (event mixing), in agreement with the expectation of an uncorrelated distribution of nucleons (Fig. 10). The p_T dependence in B_2 is still present in the results from an alternate PYTHIA 8.2 (Monash tune) simulation with color reconnection turned off (Fig. 10). Furthermore, a radial flow effect in B_2 at these low average charged multiplicities is also discarded by the EPOS (LHC) simulation with the afterburner, since this contribution only arises in high multiplicity events, starting from $dN_{ch}/d\eta > 15$ [54]. Thus, this p_T dependence can be explained as a purely hard scattering effect, in contrast to AA collisions, where it is usually attributed to collective flow.

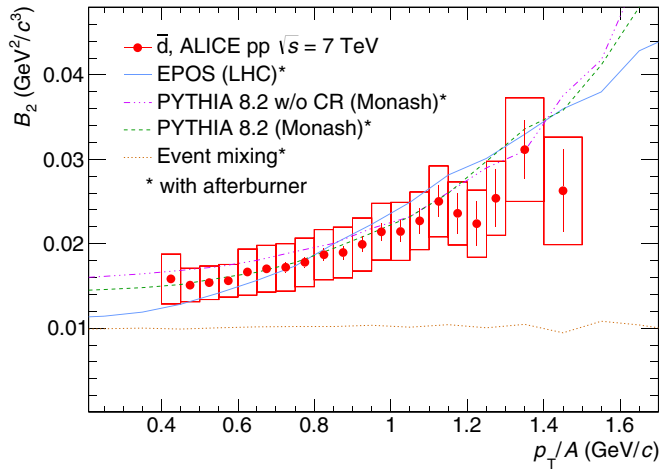

FIG. 10. Coalescence parameter (B_2) of antideuterons in inelastic pp collisions at $\sqrt{s} = 7$ TeV (circles) compared with EPOS (LHC), PYTHIA 8.2 (Monash tune) with and without color reconnection (CR), and an event mixing procedure with the afterburner (lines).

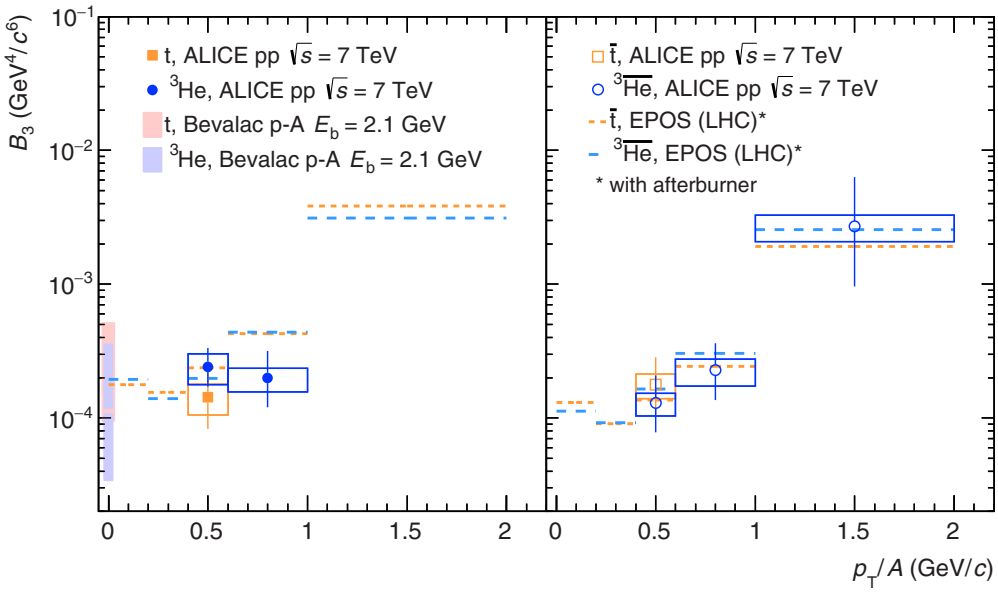

FIG. 11. Coalescence parameter (B_3) of tritons and ^{3}He nuclei (left panel) and their antinuclei (right panel) in inelastic pp collisions at $\sqrt{s} = 7$ TeV. The Bevalac measurements in p-C, p-Cu, and p-Pb collisions [1] are not given as a function of p_T and are shown as vertical bands at $p_T/A = 0$ GeV/c for comparison. Error bars and boxes represent the statistical and systematic uncertainties, respectively, and dashed lines the values obtained with EPOS (LHC) with the afterburner.

As in the case of antideuterons, the coalescence parameter (B_3) of $^3\overline{\text{He}}$ nuclei also exhibits a p_T dependence (Fig. 11 right), and can be reproduced with QCD-inspired event generators with a coalescence-based afterburner [44]. Moreover, low p_T values of B_3 are compatible with those obtained in p-C, p-Cu, and p-Pb collisions at Bevalac [1].

B. Integrated yields and deuteron-to-proton ratio

Unlike coalescence models, statistical hadronization models only provide predictions for integrated yields. In this case, the integrated yields of light nuclei and the deuteron-to-proton ratio can add additional constraints to these models and could therefore serve as a test for thermal-statistical behavior in small systems at LHC energies.

To find the integrated yields, the measurements were extrapolated to the unmeasured p_T region with a statistical distribution that provides an exponential behavior at low p_T and a power law behavior at high p_T (Figs. 5 and 7):

$$E\frac{d^3N}{dp^3} = gV\frac{m_T}{(2\pi)^3}\left(1+(q-1)\frac{m_T}{T}\right)^{\frac{q}{1-q}}, \qquad (2)$$

where $m_T = \sqrt{p_T^2 + m^2}$ is the transverse mass, and gV, T, and q are free parameters. This distribution can be derived from the Tsallis entropy [56,57] and gives good description of the data in pp collisions [57]. It was preferred over the Levy-Tsallis used in previous work [11] as it provides a more stable description of the measurements with a limited data set, as in the case of antideuterons for the center-of-mass energy 0.9 TeV or the $^3\overline{\text{He}}$ nuclei.

The systematic uncertainties of the integrated yields (dN/dy) and mean transverse momenta ($\langle p_T \rangle$) were evaluated by shifting the data points up and then down by their uncertainties (i.e., assuming full correlation between p_T bins). Additionally, the data points were shifted coherently, in a p_T-dependent way, within their uncertainties to create maximally

TABLE II. Integrated yields (dN/dy) and mean transverse momenta ($\langle p_T \rangle$) for deuterons, antideuterons, and $^3\overline{\text{He}}$ nuclei along with the extrapolated fraction (Extr.) due to the unmeasured p_T regions. The first uncertainty is the statistical uncertainty and the second one the systematic uncertainty.

	$\sqrt{s}$ (TeV)	dN/dy	$\langle p_T \rangle$ (GeV/c)	Extr.
d	0.9	$(1.12 \pm 0.09 \pm 0.09) \times 10^{-4}$	$1.01 \pm 0.05 \pm 0.05$	$50 \pm 3\%$
	2.76	$(1.53 \pm 0.05 \pm 0.13) \times 10^{-4}$	$1.04 \pm 0.02 \pm 0.04$	$45 \pm 8\%$
	7	$(2.02 \pm 0.02 \pm 0.17) \times 10^{-4}$	$1.11 \pm 0.01 \pm 0.04$	$41 \pm 5\%$
$\bar{d}$	0.9	$(1.11 \pm 0.10 \pm 0.09) \times 10^{-4}$	$0.99 \pm 0.07 \pm 0.05$	$52 \pm 7\%$
	2.76	$(1.37 \pm 0.04 \pm 0.12) \times 10^{-4}$	$1.04 \pm 0.02 \pm 0.03$	$46 \pm 7\%$
	7	$(1.92 \pm 0.02 \pm 0.15) \times 10^{-4}$	$1.08 \pm 0.01 \pm 0.04$	$42 \pm 5\%$
$^3\overline{\text{He}}$	7	$(1.1 \pm 0.6 \pm 0.2) \times 10^{-7}$	$1.6 \pm 0.4 \pm 0.04$	$43 \pm 14\%$

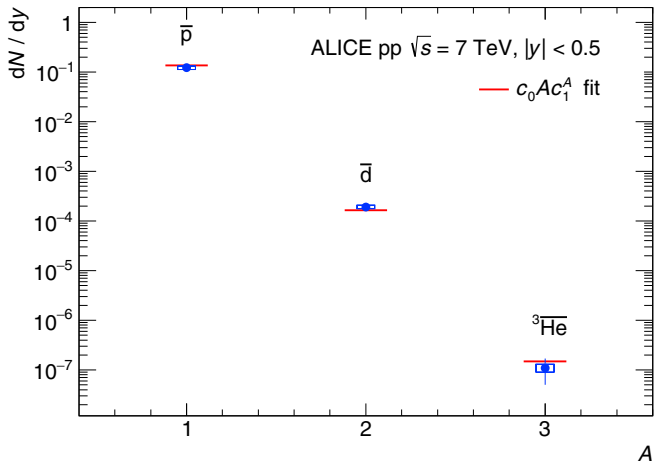

FIG. 12. Integrated yields (dN/dy) of antiprotons, antideuterons and $^3\overline{\text{He}}$ nuclei as a function of the number of antinucleons in inelastic pp collisions at $\sqrt{s} = 7$ TeV. The horizontal lines represent a fit with the function $c_0 A c_1^A$ based on Eq. (1).

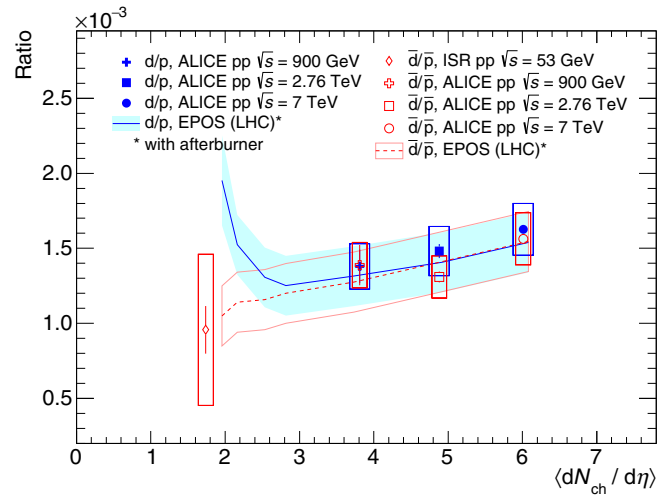

FIG. 13. Integrated deuteron-to-proton (d/p) and antideuteron-to-antiproton ($\overline{d}/\overline{p}$) ratios in inelastic pp collisions as a function of the average charged particle multiplicity for different center-of-mass energies. The average d/p ratio in AA collisions lies two times above the highest value in pp collisions (not shown). Dashed and solid lines represent the expected values from EPOS (LHC) with afterburner and the bands their uncertainties. The CERN ISR value is corrected by the contribution of feed-down antiprotons estimated with an EPOS (LHC) simulation.

hard and maximally soft p_T distributions. The values of dN/dy and $\langle p_T \rangle$ were reevaluated and the largest difference was taken as the systematic uncertainty. Table II summarizes the resulting values for the different center-of-mass energies along with the extrapolation fraction due to the unmeasured p_T regions. The uncertainty on the extrapolation was estimated by using additional distributions including the Levy-Tsallis [58,59] and Boltzmann distributions. The change of the default fit function with respect to [11] leads to slightly different values for the obtained dN/dy and $\langle p_T \rangle$ which are consistent within the respective systematic uncertainties. Figure 12 shows an exponential decrease of the dN/dy as a function of the mass number. The reduction of the yield for each additional nucleon is about 1000.

The integrated d/p and $\overline{d}/\overline{p}$ ratios were calculated from the integrated yields in Table II and Refs. [47,48], and are shown in Fig. 13 as a function of the average charged particle multiplicity at mid-rapidity [60,61]. The dN/dy values for pp collisions at the CERN ISR were computed following the same procedure described above and using the inclusive $\overline{p}$ distribution from [52] and the $\overline{d}$ distribution from Refs. [12,13]. The resulting $\overline{d}/\overline{p}$ ratio was divided by 0.69 to account for the contributions of feed-down antiprotons, based on an EPOS (LHC) simulation [44]. Figure 13 suggests an increasing trend in this ratio with the average charged particle multiplicity in pp collisions, which is also supported by an EPOS (LHC) simulation with the afterburner, although at ISR energies the d/p ratio is strongly influenced by the baryon number transport at mid-rapidity, leading to a higher value than at LHC energies according to the model expectations.

When describing particle ratios such as the d/p ratio, the only free parameter of grand-canonical statistical hadronization models at LHC energies is the chemical freeze-out temperature. In the past, several attempts were made to extend their successful description of AA collisions to smaller collision systems such as pp. In particular, the canonical formulation describes the production of light flavor hadrons, including those with strangeness content [26]. While the p/π ratio is found to be comparable in pp, p-Pb, and Pb-Pb collisions [48,62], indicating a comparable chemical freeze-out temperature among different systems, the d/p ratio in pp collisions at LHC energies is found to be two times lower than the average value in AA collisions. Since the strangeness-canonical formulation only influences the abundance of strange particles with respect to nonstrange particles, it cannot explain the observed results presented here.

VI. SUMMARY AND CONCLUSIONS

The invariant differential yields of deuterons and antideuterons in pp collisions at $\sqrt{s} = 0.9$, 2.76, and 7 TeV and the yields of tritons, ^{3}He nuclei, and their antinuclei at $\sqrt{s} = 7$ TeV have been measured in the rapidity range $|y| < 0.5$. The measurements cover the p_T ranges $0.8 < p_T < 3$ GeV/c for (anti)deuterons, $1.2 < p_T < 1.8$ GeV/c for (anti)tritons, $1.2 < p_T < 3$ GeV/c for ^{3}He nuclei and $1.2 < p_T < 6$ GeV/c for ^{3}He antinuclei. This extends previous measurements by one order of magnitude in incident energies and by a factor of 3 in p_T reach, and it includes the first ever measurements of antitritons and $^3\overline{\text{He}}$ nuclei in pp collisions.

The present measurements show no significant dependence of the coalescence parameter B_2 on the center-of-mass energy from CERN ISR energies (53 GeV) to the highest LHC energy reported in this paper (7 TeV). Moreover, the values of both B_2 and B_3 are found to be compatible at low p_T with those obtained in pA collisions at Bevalac energies.

A previously unobserved p_T dependence in pp collisions of the coalescence parameters B_2 and B_3 is also reported. The data

are well described by QCD-inspired event generators when a coalescence-based afterburner is added to take into account the momentum correlations between nucleons. According to PYTHIA 8.2 (Monash tune) and EPOS (LHC) with the afterburner, this dependence can be explained purely as a hard scattering effect.

In combination with CERN ISR measurements, our results suggest an increasing trend in the $\overline{d}/\overline{p}$ ratio with charged particle multiplicity. While the values reported in central AA collisions are in agreement with a thermal model description of particle yields, the highest d/p ratio reported in this paper is about half the thermal model value; therefore, a thermal-statistical description is disfavored in pp collisions at these low average charged particle multiplicities. Our measurements are expected to contribute to the understanding of the background from pp collisions for the observation of antideuterons and $^3\overline{\mathrm{He}}$ nuclei in cosmic ray experiments and to the estimation of the production rates of the next stable antinuclei in pp collisions.

ACKNOWLEDGMENTS

The ALICE Collaboration would like to thank all its engineers and technicians for their invaluable contributions to the construction of the experiment and the CERN accelerator teams for the outstanding performance of the LHC complex. The ALICE Collaboration gratefully acknowledges the resources and support provided by all Grid centres and the Worldwide LHC Computing Grid (WLCG) collaboration. The ALICE Collaboration acknowledges the following funding agencies for their support in building and running the ALICE detector: A. I. Alikhanyan National Science Laboratory (Yerevan Physics Institute) Foundation (ANSL), State Committee of Science and World Federation of Scientists (WFS), Armenia; Austrian Academy of Sciences and Nationalstiftung für Forschung, Technologie und Entwicklung, Austria; Ministry of Communications and High Technologies, National Nuclear Research Center, Azerbaijan; Conselho Nacional de Desenvolvimento Científico e Tecnológico (CNPq), Universidade Federal do Rio Grande do Sul (UFRGS), Financiadora de Estudos e Projetos (Finep), and Fundação de Amparo à Pesquisa do Estado de São Paulo (FAPESP), Brazil; Ministry of Science & Technology of China (MSTC), National Natural Science Foundation of China (NSFC), and Ministry of Education of China (MOEC), China; Ministry of Science, Education and Sport and Croatian Science Foundation, Croatia; Ministry of Education, Youth and Sports of the Czech Republic, Czech Republic; The Danish Council for Independent Research - Natural Sciences, the Carlsberg Foundation, and Danish National Research Foundation (DNRF), Denmark; Helsinki Institute of Physics (HIP), Finland; Commissariat à l'Energie Atomique (CEA), Institut National de Physique Nucléaire et de Physique des Particules (IN2P3), and Centre National de la Recherche Scientifique (CNRS), France; Bundesministerium für Bildung, Wissenschaft, Forschung und Technologie (BMBF), and GSI Helmholtzzentrum für Schwerionenforschung GmbH, Germany; General Secretariat for Research and Technology, Ministry of Education, Research and Religions, Greece; National Research, Development and Innovation Office, Hungary; Department of Atomic Energy Government of India (DAE), Department of Science and Technology, Government of India (DST), University Grants Commission, Government of India (UGC), and Council of Scientific and Industrial Research (CSIR), India; Indonesian Institute of Science, Indonesia; Centro Fermi - Museo Storico della Fisica e Centro Studi e Ricerche Enrico Fermi and Istituto Nazionale di Fisica Nucleare (INFN), Italy; Institute for Innovative Science and Technology, Nagasaki Institute of Applied Science (IIST), Japan Society for the Promotion of Science (JSPS) KAKENHI, and Japanese Ministry of Education, Culture, Sports, Science and Technology (MEXT), Japan; Consejo Nacional de Ciencia (CONACYT) y Tecnología, through Fondo de Cooperación Internacional en Ciencia y Tecnología (FONCICYT) and Dirección General de Asuntos del Personal Academico (DGAPA), Mexico; Nederlandse Organisatie voor Wetenschappelijk Onderzoek (NWO), Netherlands; The Research Council of Norway, Norway; Commission on Science and Technology for Sustainable Development in the South (COMSATS), Pakistan; Pontificia Universidad Católica del Perú, Peru; Ministry of Science and Higher Education and National Science Centre, Poland; Korea Institute of Science and Technology Information and National Research Foundation of Korea (NRF), Republic of Korea; Ministry of Education and Scientific Research, Institute of Atomic Physics and Romanian National Agency for Science, Technology and Innovation, Romania; Joint Institute for Nuclear Research (JINR), Ministry of Education and Science of the Russian Federation, and National Research Centre Kurchatov Institute, Russia; Ministry of Education, Science, Research and Sport of the Slovak Republic, Slovakia; National Research Foundation of South Africa, South Africa; Centro de Aplicaciones Tecnológicas y Desarrollo Nuclear (CEADEN), Cubaenergía, Cuba; Ministerio de Ciencia e Innovacion and Centro de Investigaciones Energéticas, Medioambientales y Tecnológicas (CIEMAT), Spain; Swedish Research Council (VR) and Knut & Alice Wallenberg Foundation (KAW), Sweden; European Organization for Nuclear Research, Switzerland; National Science and Technology Development Agency (NSDTA), Suranaree University of Technology (SUT), and Office of the Higher Education Commission under NRU project of Thailand, Thailand; Turkish Atomic Energy Agency (TAEK), Turkey; National Academy of Sciences of Ukraine, Ukraine; Science and Technology Facilities Council (STFC), United Kingdom; U.S. National Science Foundation (NSF) and U.S. Department of Energy, Office of Nuclear Physics (DOE NP), USA.

[1] S. Nagamiya, M.-C. Lemaire, E. Moeller, S. Schnetzer, G. Shapiro, H. Steiner, and I. Tanihata, Production of pions and light fragments at large angles in high-energy nuclear collisions, Phys. Rev. C **24**, 971 (1981).

[2] J. Barrette *et al.*, Production of light nuclei in relativistic heavy ion collisions, Phys. Rev. C **50**, 1077 (1994).

[3] N. Saito *et al.*, Composite particle production in relativistic Au+Pt, Si+Pt, and p+Pt collisions, Phys. Rev. C **49**, 3211 (1994).

[4] J. Simon-Gillo *et al.* (NA44 Collaboration), Deuteron and antideuteron production in CERN experiment NA44, Nucl. Phys. A **590**, 483 (1995).

[5] T. A. Armstrong *et al.* (E864 Collaboration), Measurements of light nuclei production in 11.5A GeV/c Au+Pb heavy-ion collisions, Phys. Rev. C **61**, 064908 (2000).

[6] T. A. Armstrong *et al.* (E864 Collaboration), Antideuteron Yield at the AGS and Coalescence Implications, Phys. Rev. Lett. **85**, 2685 (2000).

[7] S. V. Afanasiev *et al.* (NA49 Collaboration), Deuteron production in central Pb+Pb collisions at 158A GeV, Phys. Lett. B **486**, 22 (2000).

[8] S. Albergo *et al.*, Light nuclei production in heavy-ion collisions at relativistic energies, Phys. Rev. C **65**, 034907 (2002).

[9] T. Anticic *et al.* (NA49 Collaboration), Energy and centrality dependence of deuteron and proton production in Pb+Pb collisions at relativistic energies, Phys. Rev. C **69**, 024902 (2004).

[10] S. S. Adler *et al.* (PHENIX Collaboration), Deuteron and Antideuteron Production in Au+Au Collisions at $\sqrt{s_{NN}} =$ 200 GeV, Phys. Rev. Lett. **94**, 122302 (2005).

[11] J. Adam *et al.* (ALICE Collaboration), Production of light nuclei and anti-nuclei in pp and Pb-Pb collisions at energies available at the CERN Large Hadron Collider, Phys. Rev. C **93**, 024917 (2016).

[12] B. Alper *et al.* (British-Scandinavian Collaboration), Large angle production of stable particles heavier than the proton and a search for quarks at the CERN intersecting storage rings, Phys. Lett. B **46**, 265 (1973).

[13] W. M. Gibson *et al.* (British-Scandinavian-MIT Collaboration), Production of deuterons and antideuterons in proton–proton collisions at the CERN ISR, Lett. Nuovo Cimento **21**, 189 (1978).

[14] T. Alexopoulos *et al.* (Fermilab E735 Collaboration), Cross sections for deuterium, tritium, and helium production in $\overline{p}p$ collisions at $\sqrt{s} = 1.8$ TeV, Phys. Rev. D **62**, 072004 (2000).

[15] A. Aktas *et al.* (H1 Collaboration), Measurement of antideuteron photoproduction and a search for heavy stable charged particles at HERA, Eur. Phys. J. C **36**, 413 (2004).

[16] D. M. Asner *et al.* (CLEO Collaboration), Antideuteron production in $\Upsilon(nS)$ decays and the nearby continuum, Phys. Rev. D **75**, 012009 (2007).

[17] S. Schael *et al.* (ALEPH Collaboration), Deuteron and antideuteron production in e^+e^- collisions at the Z resonance, Phys. Lett. B **639**, 192 (2006).

[18] Yu. M. Antipov *et al.*, Observation of antihelium-3, Nucl. Phys. B **31**, 235 (1971).

[19] N. K. Vishnevskii *et al.*, Observation of antitritium (In Russian), Yad. Fiz. **20**, 694 (1974).

[20] G. Appelquist *et al.* (NA52 Collaboration), Antinuclei production in Pb+Pb collisions at 158 A GeV/c, Phys. Lett. B **376**, 245 (1996).

[21] C. Adler *et al.* (STAR Collaboration), $\overline{d}$ and $^3\overline{\mathrm{He}}$ Production in $\sqrt{s_{NN}} = 130$ GeV Au+Au Collisions, Phys. Rev. Lett. **87**, 262301 (2001).

[22] R. Arsenescu *et al.* (NA52 Collaboration), Antihelium-3 production in lead-lead collisions at 158 A GeV/c, New J. Phys. **5**, 1 (2003).

[23] H. Agakishiev *et al.* (STAR Collaboration), Observation of the antimatter helium-4 nucleus, Nature (Nature) **473**, 353 (2011).

[24] A. Schwarzschild and Č. Zupančič, Production of Tritons, Deuterons, Nucleons, and Mesons by 30 GeV Protons on Al, Be, and Fe Targets, Phys. Rev. **129**, 854 (1963).

[25] H. H. Gutbrod, A. Sandoval *et al.*, Final-State Interactions in the Production of Hydrogen and Helium Isotopes by Relativistic Heavy Ions on Uranium, Phys. Rev. Lett. **37**, 667 (1976).

[26] A. Andronic, P. Braun-Munzinger, J. Stachel, and H. Stöcker, Production of light nuclei, hypernuclei and their antiparticles in relativistic nuclear collisions, Phys. Lett. B **697**, 203 (2011).

[27] R. V. Wagoner, Big-bang nucleosynthesis revisited, Astrophys. J. **179**, 343 (1973).

[28] A. Kounine, The Alpha Magnetic Spectrometer on the International Space Station, Int. J. Mod. Phys. E **21**, 1230005 (2012).

[29] S. A. I. Mognet *et al.*, The prototype GAPS (pGAPS) experiment, Nucl. Instrum. Methods A **735**, 24 (2014).

[30] F. Donato, N. Fornengo, and P. Salati, Antideuterons as a signature of supersymmetric dark matter, Phys. Rev. D **62**, 043003 (2000).

[31] F. Carminati *et al.* (ALICE Collaboration), ALICE: Physics Performance Report, Volume I, J. Phys. G **30**, 1517 (2004).

[32] B. Alessandro *et al.* (ALICE Collaboration), ALICE: Physics Performance Report, Volume II, J. Phys. G **32**, 1295 (2006).

[33] K. Aamodt *et al.* (ALICE Collaboration), The ALICE experiment at the CERN LHC, J. Instrum. **3**, S08002 (2008).

[34] K. Aamodt *et al.* (ALICE Collaboration), Alignment of the ALICE Inner Tracking System with cosmic-ray tracks, J. Instrum. **5**, P03003 (2010).

[35] J. Alme *et al.*, The ALICE TPC, a large 3-dimensional tracking device with fast readout for ultra-high multiplicity events, Nucl. Instrum. Methods A **622**, 316 (2010).

[36] B. Abelev *et al.* (ALICE Collaboration), Performance of the ALICE experiment at the CERN LHC, Int. J. Mod. Phys. A **29**, 1430044 (2014).

[37] A. Akindinov *et al.*, Performance of the ALICE time-of-flight detector at the LHC, Eur. Phys. J. Plus **128**, 44 (2013).

[38] J. Adam *et al.* (ALICE Collaboration), Determination of the event collision time with the ALICE detector at the LHC, Eur. Phys. J. Plus **132**, 99 (2017).

[39] E. Abbas *et al.* (ALICE Collaboration), Performance of the ALICE VZERO system, J. Instrum. **8**, P10016 (2013).

[40] B. Abelev *et al.* (ALICE Collaboration), Measurement of inelastic, single- and double-diffraction cross sections in proton–proton collisions at the LHC with ALICE, Eur. Phys. J. C **73**, 2456 (2013).

[41] R. Brun *et al.*, GEANT, Detector Description and Simulation Tool, CERN Program Library Long Writeup W5013, 1994.

[42] H. Kamada, J. Golak, K. Miyagawa, H. Witala, and W. Glöckle, Π-mesonic decay of the hypertriton, Phys. Rev. C **57**, 1595 (1998).

[43] R. Barlow and C. Beeston, Fitting using finite Monte Carlo samples, Comput. Phys. Commun. **77**, 219 (1993).

[44] ALICE Collaboration, Supplemental material: Afterburner for generating light (anti-)nuclei with QCD-inspired event generators in pp collisions, CERN Report No. ALICE-PUBLIC-2017-010, September 2017, https://cds.cern.ch/record/2285500.

[45] B. Abelev *et al.* (ALICE Collaboration), Neutral pion and η meson production in proton–proton collisions at $\sqrt{s} = 0.9$ TeV and $\sqrt{s} = 7$ TeV, Phys. Lett. B **717**, 162 (2012).

[46] K. Aamodt *et al.* (ALICE Collaboration), Production of pions, kaons and protons in pp collisions at $\sqrt{s} = 900$ GeV with ALICE at the LHC, Eur. Phys. J. C **71**, 1655 (2011).

[47] B. Abelev *et al.* (ALICE Collaboration), Production of charged pions, kaons and protons at large transverse momenta in pp and Pb-Pb collisions at $\sqrt{s_{NN}} = 2.76$ TeV, Phys. Lett. B **736**, 196 (2014).

[48] J. Adam *et al.* (ALICE Collaboration), Measurement of pion, kaon and proton production in proton–proton collisions at $\sqrt{s} =$ 7 TeV, Eur. Phys. J. C **75**, 226 (2015).

[49] K. Aamodt *et al.* (ALICE Collaboration), Midrapidity Antiproton-to-Proton Ratio in *pp* Collisons at $\sqrt{s} = 0.9$ and 7 TeV Measured by the ALICE Experiment, Phys. Rev. Lett. **105**, 072002 (2010).

[50] E. Abbas *et al.* (ALICE Collaboration), Mid-rapidity anti-baryon to baryon ratios in pp collisions at $\sqrt{s} = 0.9$, 2.76 and 7 TeV measured by ALICE, Eur. Phys. J. C **73**, 2496 (2013).

[51] S. Chekanov *et al.* (ZEUS Collaboration), Measurement of (anti)deuteron and (anti)proton production in DIS at HERA, Nucl. Phys. B **786**, 181 (2007).

[52] B. Alper *et al.* (British-Scandinavian Collaboration), Production spectra of $\pi^{\pm}$, $K^{\pm}$, $p^{\pm}$ at large angles in proton–proton collisions in the CERN intersecting storage rings, Nucl. Phys. B **100**, 237 (1975).

[53] M. Ambrosio *et al.*, Total and elastic cross-sections and global event characteristics in $\bar{p}p$ and pp collisions at $\sqrt{s} = 53$ GeV, in *Proton-Antiproton Collider Physics - 1981*, December 1981, Madison, WI, edited by V. Barger, D. Cline, and F. Halzen, AIP Conf. Proc. No. 85 (AIP, New York, 1982), p. 602.

[54] T. Pierog, I. Karpenko, J. M. Katzy, E. Yatsenko, and K. Werner, EPOS LHC: Test of collective hadronization with data measured at the CERN Large Hadron Collider, Phys. Rev. C **92**, 034906 (2015).

[55] T. Sjöstrand, S. Mrenna, and P. Skands, A brief introduction to PYTHIA 8.1, Comput. Phys. Commun. **178**, 852 (2008).

[56] C. Tsallis, Possible generalization of Boltzmann-Gibbs statistics, J. Stat. Phys. **52**, 479 (1988).

[57] J. Cleymans and D. Worku, The Tsallis distribution in proton–proton collisions at $\sqrt{s} = 0.9$ TeV at the LHC, J. Phys. G **39**, 025006 (2012).

[58] B. I. Abelev *et al.* (STAR Collaboration), Strange particle production in p+p collisions at $\sqrt{s} = 200$ GeV, Phys. Rev. C **75**, 064901 (2007).

[59] A. Adare *et al.* (PHENIX Collaboration), Measurement of neutral mesons in p+p collisions at $\sqrt{s} = 200$ GeV and scaling properties of hadron production, Phys. Rev. D **83**, 052004 (2011).

[60] W. Thomé *et al.* (Aachen-CERN-Heidelberg-Munich Collaboration), Charged particle multiplicity distributions in pp collisions at ISR energies, Nucl. Phys. B **129**, 365 (1977).

[61] K. Aamodt *et al.* (ALICE Collaboration), Charged-particle multiplicity measurement in proton–proton collisions at $\sqrt{s}$ = 7 TeV with ALICE at LHC, Eur. Phys. J. C **68**, 345 (2010).

[62] B. Abelev *et al.* (ALICE Collaboration), Multiplicity dependence of pion, kaon, proton and lambda production in p-Pb collisions at $\sqrt{s_{NN}} = 5.02$ TeV, Phys. Lett. B **728**, 25 (2014).

S. Acharya,[137] J. Adam,[96] D. Adamová,[93] J. Adolfsson,[32] M. M. Aggarwal,[98] G. Aglieri Rinella,[33] M. Agnello,[29] N. Agrawal,[46] Z. Ahammed,[137] N. Ahmad,[15] S. U. Ahn,[78] S. Aiola,[141] A. Akindinov,[63] M. Al-Turany,[106] S. N. Alam,[137] J. L. B. Alba,[111] D. S. D. Albuquerque,[122] D. Aleksandrov,[89] B. Alessandro,[57] R. Alfaro Molina,[73] A. Alici,[11,25,52] A. Alkin,[3] J. Alme,[20] T. Alt,[69] L. Altenkamper,[20] I. Altsybeev,[136] C. Alves Garcia Prado,[121] C. Andrei,[86] D. Andreou,[33] H. A. Andrews,[110] A. Andronic,[106] V. Anguelov,[103] C. Anson,[96] T. Antičić,[107] F. Antinori,[55] P. Antonioli,[52] R. Anwar,[124] L. Aphecetche,[114] H. Appelshäuser,[69] S. Arcelli,[25] R. Arnaldi,[57] O. W. Arnold,[104,34] I. C. Arsene,[19] M. Arslandok,[103] B. Audurier,[114] A. Augustinus,[33] R. Averbeck,[106] M. D. Azmi,[15] A. Badalá,[54] Y. W. Baek,[59,77] S. Bagnasco,[57] R. Bailhache,[69] R. Bala,[100] A. Baldisseri,[74] M. Ball,[43] R. C. Baral,[66,87] A. M. Barbano,[24] R. Barbera,[26] F. Barile,[51,31] L. Barioglio,[24] G. G. Barnaföldi,[140] L. S. Barnby,[92] V. Barret,[131] P. Bartalini,[7] K. Barth,[33] E. Bartsch,[69] M. Basile,[25] N. Bastid,[131] S. Basu,[139] G. Batigne,[114] B. Batyunya,[76] P. C. Batzing,[19] I. G. Bearden,[90] H. Beck,[103] C. Bedda,[62] N. K. Behera,[59] I. Belikov,[133] F. Bellini,[25,33] H. Bello Martinez,[2] R. Bellwied,[124] L. G. E. Beltran,[120] V. Belyaev,[82] G. Bencedi,[140] S. Beole,[24] A. Bercuci,[86] Y. Berdnikov,[95] D. Berenyi,[140] R. A. Bertens,[127] D. Berzano,[33] L. Betev,[33] A. Bhasin,[100] I. R. Bhat,[100] A. K. Bhati,[98] B. Bhattacharjee,[42] J. Bhom,[118] A. Bianchi,[24] L. Bianchi,[124] N. Bianchi,[49] C. Bianchin,[139] J. Bielčík,[37] J. Bielčíková,[93] A. Bilandzic,[34,104] G. Biro,[140] R. Biswas,[4] S. Biswas,[4] J. T. Blair,[119] D. Blau,[89] C. Blume,[69] G. Boca,[134] F. Bock,[103,81,33] A. Bogdanov,[82] L. Boldizsár,[140] M. Bombara,[38] G. Bonomi,[135] M. Bonora,[33] J. Book,[69] H. Borel,[74] A. Borissov,[17,103] M. Borri,[126] E. Botta,[24] C. Bourjau,[90] L. Bratrud,[69] P. Braun-Munzinger,[106] M. Bregant,[121] T. A. Broker,[69] M. Broz,[37] E. J. Brucken,[44] E. Bruna,[57] G. E. Bruno,[33,31] D. Budnikov,[108] H. Buesching,[69] S. Bufalino,[29] P. Buhler,[113] P. Buncic,[33] O. Busch,[130] Z. Buthelezi,[75] J. B. Butt,[14] J. T. Buxton,[16] J. Cabala,[116] D. Caffarri,[33,91] H. Caines,[141] A. Caliva,[62,106] E. Calvo Villar,[111] P. Camerini,[23] A. A. Capon,[113] F. Carena,[33] W. Carena,[33] F. Carnesecchi,[25,11] J. Castillo Castellanos,[74] A. J. Castro,[127] E. A. R. Casula,[53] C. Ceballos Sanchez,[9] P. Cerello,[57] S. Chandra,[137] B. Chang,[125] S. Chapeland,[33] M. Chartier,[126] S. Chattopadhyay,[137] S. Chattopadhyay,[109] A. Chauvin,[34,104] C. Cheshkov,[132] B. Cheynis,[132] V. Chibante Barroso,[33] D. D. Chinellato,[122] S. Cho,[59] P. Chochula,[33] M. Chojnacki,[90] S. Choudhury,[137] T. Chowdhury,[131] P. Christakoglou,[91] C. H. Christensen,[90] P. Christiansen,[32] T. Chujo,[130] S. U. Chung,[17] C. Cicalo,[53] L. Cifarelli,[11,25] F. Cindolo,[52] J. Cleymans,[99] F. Colamaria,[31] D. Colella,[33,64,51] A. Collu,[81] M. Colocci,[25] M. Concas,[57,*] G. Conesa Balbastre,[80] Z. Conesa del Valle,[60] M. E. Connors,[141,†] J. G. Contreras,[37] T. M. Cormier,[94] Y. Corrales Morales,[57] I. Cortés Maldonado,[2] P. Cortese,[30] M. R. Cosentino,[123] F. Costa,[33] S. Costanza,[134] J. Crkovská,[60] P. Crochet,[131] E. Cuautle,[71] L. Cunqueiro,[70] T. Dahms,[34,104] A. Dainese,[55] M. C. Danisch,[103] A. Danu,[67]

D. Das,[109] I. Das,[109] S. Das,[4] A. Dash,[87] S. Dash,[46] S. De,[47,121] A. De Caro,[28] G. de Cataldo,[51] C. de Conti,[121] J. de Cuveland,[40] A. De Falco,[22] D. De Gruttola,[28,11] N. De Marco,[57] S. De Pasquale,[28] R. D. De Souza,[122] H. F. Degenhardt,[121] A. Deisting,[106,103] A. Deloff,[85] C. Deplano,[91] P. Dhankher,[46] D. Di Bari,[31] A. Di Mauro,[33] P. Di Nezza,[49] B. Di Ruzza,[55] T. Dietel,[99] P. Dillenseger,[69] R. Divià,[33] Ø. Djuvsland,[20] A. Dobrin,[33] D. Domenicis Gimenez,[121] B. Dönigus,[69] O. Dordic,[19] L. V. R. Doremalen,[62] A. K. Dubey,[137] A. Dubla,[106] L. Ducroux,[132] A. K. Duggal,[98] M. Dukhishyam,[87] P. Dupieux,[131] R. J. Ehlers,[141] D. Elia,[51] E. Endress,[111] H. Engel,[68] E. Epple,[141] B. Erazmus,[114] F. Erhardt,[97] B. Espagnon,[60] S. Esumi,[130] G. Eulisse,[33] J. Eum,[17] D. Evans,[110] S. Evdokimov,[112] L. Fabbietti,[104,34] J. Faivre,[80] A. Fantoni,[49] M. Fasel,[94,81] L. Feldkamp,[70] A. Feliciello,[57] G. Feofilov,[136] A. Fernández Téllez,[2] A. Ferretti,[24] A. Festanti,[27,33] V. J. G. Feuillard,[74,131] J. Figiel,[118] M. A. S. Figueredo,[121] S. Filchagin,[108] D. Finogeev,[61] F. M. Fionda,[20,22] M. Floris,[33] S. Foertsch,[75] P. Foka,[106] S. Fokin,[89] E. Fragiacomo,[58] A. Francescon,[33] A. Francisco,[114] U. Frankenfeld,[106] G. G. Fronze,[24] U. Fuchs,[33] C. Furget,[80] A. Furs,[61] M. Fusco Girard,[28] J. J. Gaardhøje,[90] M. Gagliardi,[24] A. M. Gago,[111] K. Gajdosova,[90] M. Gallio,[24] C. D. Galvan,[120] P. Ganoti,[84] C. Garabatos,[106] E. Garcia-Solis,[12] K. Garg,[26] C. Gargiulo,[33] P. Gasik,[104,34] E. F. Gauger,[119] M. B. Gay Ducati,[72] M. Germain,[114] J. Ghosh,[109] P. Ghosh,[137] S. K. Ghosh,[4] P. Gianotti,[49] P. Giubellino,[33,106,57] P. Giubilato,[27] E. Gladysz-Dziadus,[118] P. Glässel,[103] D. M. Gomëz Coral,[73] A. Gomez Ramirez,[68] A. S. Gonzalez,[33] P. González-Zamora,[2] S. Gorbunov,[40] L. Görlich,[118] S. Gotovac,[117] V. Grabski,[73] L. K. Graczykowski,[138] K. L. Graham,[110] L. Greiner,[81] A. Grelli,[62] C. Grigoras,[33] V. Grigoriev,[82] A. Grigoryan,[1] S. Grigoryan,[76] J. M. Gronefeld,[106] F. Grosa,[29] J. F. Grosse-Oetringhaus,[33] R. Grosso,[106] L. Gruber,[113] F. Guber,[61] R. Guernane,[80] B. Guerzoni,[25] K. Gulbrandsen,[90] T. Gunji,[129] A. Gupta,[100] R. Gupta,[100] I. B. Guzman,[2] R. Haake,[33] C. Hadjidakis,[60] H. Hamagaki,[83] G. Hamar,[140] J. C. Hamon,[133] M. R. Haque,[62] J. W. Harris,[141] A. Harton,[12] H. Hassan,[80] D. Hatzifotiadou,[11,52] S. Hayashi,[129] S. T. Heckel,[69] E. Hellbär,[69] H. Helstrup,[35] A. Herghelegiu,[86] E. G. Hernandez,[2] G. Herrera Corral,[10] F. Herrmann,[70] B. A. Hess,[102] K. F. Hetland,[35] H. Hillemanns,[33] C. Hills,[126] B. Hippolyte,[133] J. Hladky,[65] B. Hohlweger,[104] D. Horak,[37] S. Hornung,[106] R. Hosokawa,[130,80] P. Hristov,[33] C. Hughes,[127] T. J. Humanic,[16] N. Hussain,[42] T. Hussain,[15] D. Hutter,[40] D. S. Hwang,[18] S. A. Iga Buitron,[71] R. Ilkaev,[108] M. Inaba,[130] M. Ippolitov,[82,89] M. Irfan,[15] M. S. Islam,[109] M. Ivanov,[106] V. Ivanov,[95] V. Izucheev,[112] B. Jacak,[81] N. Jacazio,[25] P. M. Jacobs,[81] M. B. Jadhav,[46] J. Jadlovsky,[116] S. Jaelani,[62] C. Jahnke,[34] M. J. Jakubowska,[138] M. A. Janik,[138] P. H. S. Y. Jayarathna,[124] C. Jena,[87] S. Jena,[124] M. Jercic,[97] R. T. Jimenez Bustamante,[106] P. G. Jones,[110] A. Jusko,[110] P. Kalinak,[64] A. Kalweit,[33] J. H. Kang,[142] V. Kaplin,[82] S. Kar,[137] A. Karasu Uysal,[79] O. Karavichev,[61] T. Karavicheva,[61] L. Karayan,[103,106] P. Karczmarczyk,[33] E. Karpechev,[61] U. Kebschull,[68] R. Keidel,[143] D. L. D. Keijdener,[62] M. Keil,[33] B. Ketzer,[43] Z. Khabanova,[91] P. Khan,[109] S. A. Khan,[137] A. Khanzadeev,[95] Y. Kharlov,[112] A. Khatun,[15] A. Khuntia,[47] M. M. Kielbowicz,[118] B. Kileng,[35] B. Kim,[130] D. Kim,[142] D. J. Kim,[125] H. Kim,[142] J. S. Kim,[41] J. Kim,[103] M. Kim,[59] M. Kim,[142] S. Kim,[18] T. Kim,[142] S. Kirsch,[40] I. Kisel,[40] S. Kiselev,[63] A. Kisiel,[138] G. Kiss,[140] J. L. Klay,[6] C. Klein,[69] J. Klein,[33] C. Klein-Bösing,[70] S. Klewin,[103] A. Kluge,[33] M. L. Knichel,[33,103] A. G. Knospe,[124] C. Kobdaj,[115] M. Kofarago,[140] M. K. Köhler,[103] T. Kollegger,[106] V. Kondratiev,[136] N. Kondratyeva,[82] E. Kondratyuk,[112] A. Konevskikh,[61] M. Konyushikhin,[139] M. Kopcik,[116] M. Kour,[100] C. Kouzinopoulos,[33] O. Kovalenko,[85] V. Kovalenko,[136] M. Kowalski,[118] G. Koyithatta Meethaleveedu,[46] I. Králik,[64] A. Kravčáková,[38] L. Kreis,[106] M. Krivda,[110,64] F. Krizek,[93] E. Kryshen,[95] M. Krzewicki,[40] A. M. Kubera,[16] V. Kučera,[93] C. Kuhn,[133] P. G. Kuijer,[91] A. Kumar,[100] J. Kumar,[46] L. Kumar,[98] S. Kumar,[46] S. Kundu,[87] P. Kurashvili,[85] A. Kurepin,[61] A. B. Kurepin,[61] A. Kuryakin,[108] S. Kushpil,[93] M. J. Kweon,[59] Y. Kwon,[142] S. L. La Pointe,[40] P. La Rocca,[26] C. Lagana Fernandes,[121] Y. S. Lai,[81] I. Lakomov,[33] R. Langoy,[39] K. Lapidus,[141] C. Lara,[68] A. Lardeux,[74,19] A. Lattuca,[24] E. Laudi,[33] R. Lavicka,[37] R. Lea,[23] L. Leardini,[103] S. Lee,[142] F. Lehas,[91] S. Lehner,[113] J. Lehrbach,[40] R. C. Lemmon,[92] V. Lenti,[51] E. Leogrande,[62] I. León Monzón,[120] P. Lévai,[140] X. Li,[13] J. Lien,[39] R. Lietava,[110] B. Lim,[17] S. Lindal,[19] V. Lindenstruth,[40] S. W. Lindsay,[126] C. Lippmann,[106] M. A. Lisa,[16] V. Litichevskyi,[44] W. J. Llope,[139] D. F. Lodato,[62] P. I. Loenne,[20] V. Loginov,[82] C. Loizides,[81] P. Loncar,[117] X. Lopez,[131] E. López Torres,[9] A. Lowe,[140] P. Luettig,[69] J. R. Luhder,[70] M. Lunardon,[27] G. Luparello,[58,23] M. Lupi,[33] T. H. Lutz,[141] A. Maevskaya,[61] M. Mager,[33] S. Mahajan,[100] S. M. Mahmood,[19] A. Maire,[133] R. D. Majka,[141] M. Malaev,[95] L. Malinina,[76,‡] D. Mal'Kevich,[63] P. Malzacher,[106] A. Mamonov,[108] V. Manko,[89] F. Manso,[131] V. Manzari,[51] Y. Mao,[7] M. Marchisone,[75,128] J. Mareš,[65] G. V. Margagliotti,[23] A. Margotti,[52] J. Margutti,[62] A. Marín,[106] C. Markert,[119] M. Marquard,[69] N. A. Martin,[106] P. Martinengo,[33] J. A. L. Martinez,[68] M. I. Martínez,[2] G. Martínez García,[114] M. Martinez Pedreira,[33] S. Masciocchi,[106] M. Masera,[24] A. Masoni,[53] E. Masson,[114] A. Mastroserio,[51] A. M. Mathis,[104,34] P. F. T. Matuoka,[121] A. Matyja,[127] C. Mayer,[118] J. Mazer,[127] M. Mazzilli,[31] M. A. Mazzoni,[56] F. Meddi,[21] Y. Melikyan,[82] A. Menchaca-Rocha,[73] E. Meninno,[28] J. Mercado Pérez,[103] M. Meres,[36] S. Mhlanga,[99] Y. Miake,[130] M. M. Mieskolainen,[44] D. L. Mihaylov,[104] K. Mikhaylov,[63,76] J. Milosevic,[19] A. Mischke,[62] A. N. Mishra,[47] D. Miśkowiec,[106] J. Mitra,[137] C. M. Mitu,[67] N. Mohammadi,[62] B. Mohanty,[87] M. Mohisin Khan,[15,§] D. A. Moreira De Godoy,[70] L. A. P. Moreno,[2] S. Moretto,[27] A. Morreale,[114] A. Morsch,[33] V. Muccifora,[49] E. Mudnic,[117] D. Mühlheim,[70] S. Muhuri,[137] M. Mukherjee,[4] J. D. Mulligan,[141] M. G. Munhoz,[121] K. Münning,[43] R. H. Munzer,[69] H. Murakami,[129] S. Murray,[75] L. Musa,[33] J. Musinsky,[64] C. J. Myers,[124] J. W. Myrcha,[138] D. Nag,[4] B. Naik,[46] R. Nair,[85] B. K. Nandi,[46] R. Nania,[52,11] E. Nappi,[51] A. Narayan,[46] M. U. Naru,[14] H. Natal da Luz,[121] C. Nattrass,[127] S. R. Navarro,[2] K. Nayak,[87] R. Nayak,[46] T. K. Nayak,[137] S. Nazarenko,[108] A. Nedosekin,[63] R. A. Negrao De Oliveira,[33] L. Nellen,[71] S. V. Nesbo,[35] F. Ng,[124] M. Nicassio,[106] M. Niculescu,[67] J. Niedziela,[138,33] B. S. Nielsen,[90] S. Nikolaev,[89] S. Nikulin,[89] V. Nikulin,[95] F. Noferini,[11,52] P. Nomokonov,[76] G. Nooren,[62] J. C. C. Noris,[2] J. Norman,[126] A. Nyanin,[89] J. Nystrand,[20] H. Oeschler,[17,103,‖] S. Oh,[141] A. Ohlson,[33,103] T. Okubo,[45] L. Olah,[140] J. Oleniacz,[138] A. C. Oliveira Da Silva,[121] M. H. Oliver,[141] J. Onderwaater,[106] C. Oppedisano,[57] R. Orava,[44] M. Oravec,[116]

A. Ortiz Velasquez,[71] A. Oskarsson,[32] J. Otwinowski,[118] K. Oyama,[83] Y. Pachmayer,[103] V. Pacik,[90] D. Pagano,[135] P. Pagano,[28] G. Paić,[71] P. Palni,[7] J. Pan,[139] A. K. Pandey,[46] S. Panebianco,[74] V. Papikyan,[1] G. S. Pappalardo,[54] P. Pareek,[47] J. Park,[59] S. Parmar,[98] A. Passfeld,[70] S. P. Pathak,[124] R. N. Patra,[137] B. Paul,[57] H. Pei,[7] T. Peitzmann,[62] X. Peng,[7] L. G. Pereira,[72] H. Pereira Da Costa,[74] D. Peresunko,[89,82] E. Perez Lezama,[69] V. Peskov,[69] Y. Pestov,[5] V. Petráček,[37] V. Petrov,[112] M. Petrovici,[86] C. Petta,[26] R. P. Pezzi,[72] S. Piano,[58] M. Pikna,[36] P. Pillot,[114] L. O. D. L. Pimentel,[90] O. Pinazza,[52,33] L. Pinsky,[124] D. B. Piyarathna,[124] M. Płoskoń,[81] M. Planinic,[97] F. Pliquett,[69] J. Pluta,[138] S. Pochybova,[140] P. L. M. Podesta-Lerma,[120] M. G. Poghosyan,[94] B. Polichtchouk,[112] N. Poljak,[97] W. Poonsawat,[115] A. Pop,[86] H. Poppenborg,[70] S. Porteboeuf-Houssais,[131] V. Pozdniakov,[76] S. K. Prasad,[4] R. Preghenella,[52] F. Prino,[57] C. A. Pruneau,[139] I. Pshenichnov,[61] M. Puccio,[24] G. Puddu,[22] P. Pujahari,[139] V. Punin,[108] J. Putschke,[139] S. Raha,[4] S. Rajput,[100] J. Rak,[125] A. Rakotozafindrabe,[74] L. Ramello,[30] F. Rami,[133] D. B. Rana,[124] R. Raniwala,[101] S. Raniwala,[101] S. S. Räsänen,[44] B. T. Rascanu,[69] D. Rathee,[98] V. Ratza,[43] I. Ravasenga,[29] K. F. Read,[127,94] K. Redlich,[85,¶] A. Rehman,[20] P. Reichelt,[69] F. Reidt,[33] X. Ren,[7] R. Renfordt,[69] A. R. Reolon,[49] A. Reshetin,[61] K. Reygers,[103] V. Riabov,[95] R. A. Ricci,[50] T. Richert,[32] M. Richter,[19] P. Riedler,[33] W. Riegler,[33] F. Riggi,[26] C. Ristea,[67] M. Rodríguez Cahuantzi,[2] K. Røed,[19] E. Rogochaya,[76] D. Rohr,[33,40] D. Röhrich,[20] P. S. Rokita,[138] F. Ronchetti,[49] E. D. Rosas,[71] P. Rosnet,[131] A. Rossi,[27,55] A. Rotondi,[134] F. Roukoutakis,[84] A. Roy,[47] C. Roy,[133] P. Roy,[109] O. V. Rueda,[71] R. Rui,[23] B. Rumyantsev,[76] A. Rustamov,[88] E. Ryabinkin,[89] Y. Ryabov,[95] A. Rybicki,[118] S. Saarinen,[44] S. Sadhu,[137] S. Sadovsky,[112] K. Šafařík,[33] S. K. Saha,[137] B. Sahlmuller,[69] B. Sahoo,[46] P. Sahoo,[47] R. Sahoo,[47] S. Sahoo,[66] P. K. Sahu,[66] J. Saini,[137] S. Sakai,[130] M. A. Saleh,[139] J. Salzwedel,[16] S. Sambyal,[100] V. Samsonov,[95,82] A. Sandoval,[73] D. Sarkar,[137] N. Sarkar,[137] P. Sarma,[42] M. H. P. Sas,[62] E. Scapparone,[52] F. Scarlassara,[27] B. Schaefer,[94] R. P. Scharenberg,[105] H. S. Scheid,[69] C. Schiaua,[86] R. Schicker,[103] C. Schmidt,[106] H. R. Schmidt,[102] M. O. Schmidt,[103] M. Schmidt,[102] N. V. Schmidt,[94,69] J. Schukraft,[33] Y. Schutz,[33,133] K. Schwarz,[106] K. Schweda,[106] G. Scioli,[25] E. Scomparin,[57] M. Šefčík,[38] J. E. Seger,[96] Y. Sekiguchi,[129] D. Sekihata,[45] I. Selyuzhenkov,[106,82] K. Senosi,[75] S. Senyukov,[3,133,33] E. Serradilla,[73] P. Sett,[46] A. Sevcenco,[67] A. Shabanov,[61] A. Shabetai,[114] R. Shahoyan,[33] W. Shaikh,[109] A. Shangaraev,[112] A. Sharma,[98] A. Sharma,[100] M. Sharma,[100] M. Sharma,[100] N. Sharma,[98,127] A. I. Sheikh,[137] K. Shigaki,[45] Q. Shou,[7] K. Shtejer,[9,24] Y. Sibiriak,[89] S. Siddhanta,[53] K. M. Sielewicz,[33] T. Siemiarczuk,[85] S. Silaeva,[89] D. Silvermyr,[32] C. Silvestre,[80] G. Simatovic,[97] G. Simonetti,[33] R. Singaraju,[137] R. Singh,[87] V. Singhal,[137] T. Sinha,[109] B. Sitar,[36] M. Sitta,[30] T. B. Skaali,[19] M. Slupecki,[125] N. Smirnov,[141] R. J. M. Snellings,[62] T. W. Snellman,[125] J. Song,[17] M. Song,[142] F. Soramel,[27] S. Sorensen,[127] F. Sozzi,[106] E. Spiriti,[49] I. Sputowska,[118] B. K. Srivastava,[105] J. Stachel,[103] I. Stan,[67] P. Stankus,[94] E. Stenlund,[32] D. Stocco,[114] M. M. Storetvedt,[35] P. Strmen,[36] A. A. P. Suaide,[121] T. Sugitate,[45] C. Suire,[60] M. Suleymanov,[14] M. Suljic,[23] R. Sultanov,[63] M. Šumbera,[93] S. Sumowidagdo,[48] K. Suzuki,[113] S. Swain,[66] A. Szabo,[36] I. Szarka,[36] U. Tabassam,[14] J. Takahashi,[122] G. J. Tambave,[20] N. Tanaka,[130] M. Tarhini,[60] M. Tariq,[15] M. G. Tarzila,[86] A. Tauro,[33] G. Tejeda Muñoz,[2] A. Telesca,[33] K. Terasaki,[129] C. Terrevoli,[27] B. Teyssier,[132] D. Thakur,[47] S. Thakur,[137] D. Thomas,[119] F. Thoresen,[90] R. Tieulent,[132] A. Tikhonov,[61] A. R. Timmins,[124] A. Toia,[69] S. R. Torres,[120] S. Tripathy,[47] S. Trogolo,[24] G. Trombetta,[31] L. Tropp,[38] V. Trubnikov,[3] W. H. Trzaska,[125] B. A. Trzeciak,[62] T. Tsuji,[129] A. Tumkin,[108] R. Turrisi,[55] T. S. Tveter,[19] K. Ullaland,[20] E. N. Umaka,[124] A. Uras,[132] G. L. Usai,[22] A. Utrobicic,[97] M. Vala,[116,64] J. Van Der Maarel,[62] J. W. Van Hoorne,[33] M. van Leeuwen,[62] T. Vanat,[93] P. Vande Vyvre,[33] D. Varga,[140] A. Vargas,[2] M. Vargyas,[125] R. Varma,[46] M. Vasileiou,[84] A. Vasiliev,[89] A. Vauthier,[80] O. Vázquez Doce,[104,34] V. Vechernin,[136] A. M. Veen,[62] A. Velure,[20] E. Vercellin,[24] S. Vergara Limón,[2] R. Vernet,[8] R. Vértesi,[140] L. Vickovic,[117] S. Vigolo,[62] J. Viinikainen,[125] Z. Vilakazi,[128] O. Villalobos Baillie,[110] A. Villatoro Tello,[2] A. Vinogradov,[89] L. Vinogradov,[136] T. Virgili,[28] V. Vislavicius,[32] A. Vodopyanov,[76] M. A. Völkl,[103,102] K. Voloshin,[63] S. A. Voloshin,[139] G. Volpe,[31] B. von Haller,[33] I. Vorobyev,[104,34] D. Voscek,[116] D. Vranic,[33,106] J. Vrláková,[38] B. Wagner,[20] H. Wang,[62] M. Wang,[7] D. Watanabe,[130] Y. Watanabe,[129,130] M. Weber,[113] S. G. Weber,[106] D. F. Weiser,[103] S. C. Wenzel,[33] J. P. Wessels,[70] U. Westerhoff,[70] A. M. Whitehead,[99] J. Wiechula,[69] J. Wikne,[19] G. Wilk,[85] J. Wilkinson,[103,52] G. A. Willems,[70] M. C. S. Williams,[52] E. Willsher,[110] B. Windelband,[103] W. E. Witt,[127] S. Yalcin,[79] K. Yamakawa,[45] P. Yang,[7] S. Yano,[45] Z. Yin,[7] H. Yokoyama,[130,80] I.-K. Yoo,[17] J. H. Yoon,[59] V. Yurchenko,[3] V. Zaccolo,[57] A. Zaman,[14] C. Zampolli,[33] H. J. C. Zanoli,[121] N. Zardoshti,[110] A. Zarochentsev,[136] P. Závada,[65] N. Zaviyalov,[108] H. Zbroszczyk,[138] M. Zhalov,[95] H. Zhang,[20,7] X. Zhang,[7] Y. Zhang,[7] C. Zhang,[62] Z. Zhang,[7,131] C. Zhao,[19] N. Zhigareva,[63] D. Zhou,[7] Y. Zhou,[90] Z. Zhou,[20] H. Zhu,[20] J. Zhu,[7] A. Zichichi,[25,11] A. Zimmermann,[103] M. B. Zimmermann,[33] G. Zinovjev,[3] J. Zmeskal,[113] and S. Zou[7]

(ALICE Collaboration)

[1]*A. I. Alikhanyan National Science Laboratory (Yerevan Physics Institute) Foundation, Yerevan, Armenia*
[2]*Benemérita Universidad Autónoma de Puebla, Puebla, Mexico*
[3]*Bogolyubov Institute for Theoretical Physics, Kiev, Ukraine*
[4]*Bose Institute, Department of Physics and Centre for Astroparticle Physics and Space Science (CAPSS), Kolkata, India*
[5]*Budker Institute for Nuclear Physics, Novosibirsk, Russia*
[6]*California Polytechnic State University, San Luis Obispo, California, USA*
[7]*Central China Normal University, Wuhan, China*
[8]*Centre de Calcul de l'IN2P3, Villeurbanne, Lyon, France*
[9]*Centro de Aplicaciones Tecnológicas y Desarrollo Nuclear (CEADEN), Havana, Cuba*

[10]*Centro de Investigación y de Estudios Avanzados (CINVESTAV), Mexico City and Mérida, Mexico*
[11]*Centro Fermi - Museo Storico della Fisica e Centro Studi e Ricerche "Enrico Fermi", Rome, Italy*
[12]*Chicago State University, Chicago, Illinois, USA*
[13]*China Institute of Atomic Energy, Beijing, China*
[14]*COMSATS Institute of Information Technology (CIIT), Islamabad, Pakistan*
[15]*Department of Physics, Aligarh Muslim University, Aligarh, India*
[16]*Department of Physics, Ohio State University, Columbus, Ohio, USA*
[17]*Department of Physics, Pusan National University, Pusan, Republic of Korea*
[18]*Department of Physics, Sejong University, Seoul, Republic of Korea*
[19]*Department of Physics, University of Oslo, Oslo, Norway*
[20]*Department of Physics and Technology, University of Bergen, Bergen, Norway*
[21]*Dipartimento di Fisica dell'Università "La Sapienza" and Sezione INFN, Rome, Italy*
[22]*Dipartimento di Fisica dell'Università and Sezione INFN, Cagliari, Italy*
[23]*Dipartimento di Fisica dell'Università and Sezione INFN, Trieste, Italy*
[24]*Dipartimento di Fisica dell'Università and Sezione INFN, Turin, Italy*
[25]*Dipartimento di Fisica e Astronomia dell'Università and Sezione INFN, Bologna, Italy*
[26]*Dipartimento di Fisica e Astronomia dell'Università and Sezione INFN, Catania, Italy*
[27]*Dipartimento di Fisica e Astronomia dell'Università and Sezione INFN, Padova, Italy*
[28]*Dipartimento di Fisica "E. R. Caianiello" dell'Università and Gruppo Collegato INFN, Salerno, Italy*
[29]*Dipartimento DISAT del Politecnico and Sezione INFN, Turin, Italy*
[30]*Dipartimento di Scienze e Innovazione Tecnologica dell'Università del Piemonte Orientale and INFN Sezione di Torino, Alessandria, Italy*
[31]*Dipartimento Interateneo di Fisica "M. Merlin" and Sezione INFN, Bari, Italy*
[32]*Division of Experimental High Energy Physics, University of Lund, Lund, Sweden*
[33]*European Organization for Nuclear Research (CERN), Geneva, Switzerland*
[34]*Excellence Cluster Universe, Technische Universität München, Munich, Germany*
[35]*Faculty of Engineering, Bergen University College, Bergen, Norway*
[36]*Faculty of Mathematics, Physics and Informatics, Comenius University, Bratislava, Slovakia*
[37]*Faculty of Nuclear Sciences and Physical Engineering, Czech Technical University in Prague, Prague, Czech Republic*
[38]*Faculty of Science, P. J. Šafárik University, Košice, Slovakia*
[39]*Faculty of Technology, Buskerud and Vestfold University College, Tonsberg, Norway*
[40]*Frankfurt Institute for Advanced Studies, Johann Wolfgang Goethe-Universität Frankfurt, Frankfurt, Germany*
[41]*Gangneung-Wonju National University, Gangneung, Republic of Korea*
[42]*Gauhati University, Department of Physics, Guwahati, India*
[43]*Helmholtz-Institut für Strahlen- und Kernphysik, Rheinische Friedrich-Wilhelms-Universität Bonn, Bonn, Germany*
[44]*Helsinki Institute of Physics (HIP), Helsinki, Finland*
[45]*Hiroshima University, Hiroshima, Japan*
[46]*Indian Institute of Technology Bombay (IIT), Mumbai, India*
[47]*Indian Institute of Technology Indore, Indore, India*
[48]*Indonesian Institute of Sciences, Jakarta, Indonesia*
[49]*INFN, Laboratori Nazionali di Frascati, Frascati, Italy*
[50]*INFN, Laboratori Nazionali di Legnaro, Legnaro, Italy*
[51]*INFN, Sezione di Bari, Bari, Italy*
[52]*INFN, Sezione di Bologna, Bologna, Italy*
[53]*INFN, Sezione di Cagliari, Cagliari, Italy*
[54]*INFN, Sezione di Catania, Catania, Italy*
[55]*INFN, Sezione di Padova, Padova, Italy*
[56]*INFN, Sezione di Roma, Rome, Italy*
[57]*INFN, Sezione di Torino, Turin, Italy*
[58]*INFN, Sezione di Trieste, Trieste, Italy*
[59]*Inha University, Incheon, Republic of Korea*
[60]*Institut de Physique Nucléaire d'Orsay (IPNO), Université Paris-Sud, CNRS-IN2P3, Orsay, France*
[61]*Institute for Nuclear Research, Academy of Sciences, Moscow, Russia*
[62]*Institute for Subatomic Physics of Utrecht University, Utrecht, Netherlands*
[63]*Institute for Theoretical and Experimental Physics, Moscow, Russia*
[64]*Institute of Experimental Physics, Slovak Academy of Sciences, Košice, Slovakia*
[65]*Institute of Physics, Academy of Sciences of the Czech Republic, Prague, Czech Republic*
[66]*Institute of Physics, Bhubaneswar, India*
[67]*Institute of Space Science (ISS), Bucharest, Romania*
[68]*Institut für Informatik, Johann Wolfgang Goethe-Universität Frankfurt, Frankfurt, Germany*

[69]*Institut für Kernphysik, Johann Wolfgang Goethe-Universität Frankfurt, Frankfurt, Germany*
[70]*Institut für Kernphysik, Westfälische Wilhelms-Universität Münster, Münster, Germany*
[71]*Instituto de Ciencias Nucleares, Universidad Nacional Autónoma de México, Mexico City, Mexico*
[72]*Instituto de Física, Universidade Federal do Rio Grande do Sul (UFRGS), Porto Alegre, Brazil*
[73]*Instituto de Física, Universidad Nacional Autónoma de México, Mexico City, Mexico*
[74]*IRFU, CEA, Université Paris-Saclay, Saclay, France*
[75]*iThemba LABS, National Research Foundation, Somerset West, South Africa*
[76]*Joint Institute for Nuclear Research (JINR), Dubna, Russia*
[77]*Konkuk University, Seoul, Republic of Korea*
[78]*Korea Institute of Science and Technology Information, Daejeon, Republic of Korea*
[79]*KTO Karatay University, Konya, Turkey*
[80]*Laboratoire de Physique Subatomique et de Cosmologie, Université Grenoble-Alpes, CNRS-IN2P3, Grenoble, France*
[81]*Lawrence Berkeley National Laboratory, Berkeley, California, USA*
[82]*Moscow Engineering Physics Institute, Moscow, Russia*
[83]*Nagasaki Institute of Applied Science, Nagasaki, Japan*
[84]*National and Kapodistrian University of Athens, Physics Department, Athens, Greece*
[85]*National Centre for Nuclear Studies, Warsaw, Poland*
[86]*National Institute for Physics and Nuclear Engineering, Bucharest, Romania*
[87]*National Institute of Science Education and Research, HBNI, Jatni, India*
[88]*National Nuclear Research Center, Baku, Azerbaijan*
[89]*National Research Centre Kurchatov Institute, Moscow, Russia*
[90]*Niels Bohr Institute, University of Copenhagen, Copenhagen, Denmark*
[91]*Nikhef, Nationaal instituut voor subatomaire fysica, Amsterdam, Netherlands*
[92]*Nuclear Physics Group, STFC Daresbury Laboratory, Daresbury, United Kingdom*
[93]*Nuclear Physics Institute, Academy of Sciences of the Czech Republic, Řež u Prahy, Czech Republic*
[94]*Oak Ridge National Laboratory, Oak Ridge, Tennessee, USA*
[95]*Petersburg Nuclear Physics Institute, Gatchina, Russia*
[96]*Physics Department, Creighton University, Omaha, Nebraska, USA*
[97]*Physics department, Faculty of Science, University of Zagreb, Zagreb, Croatia*
[98]*Physics Department, Panjab University, Chandigarh, India*
[99]*Physics Department, University of Cape Town, Cape Town, South Africa*
[100]*Physics Department, University of Jammu, Jammu, India*
[101]*Physics Department, University of Rajasthan, Jaipur, India*
[102]*Physikalisches Institut, Eberhard Karls Universität Tübingen, Tübingen, Germany*
[103]*Physikalisches Institut, Ruprecht-Karls-Universität Heidelberg, Heidelberg, Germany*
[104]*Physik Department, Technische Universität München, Munich, Germany*
[105]*Purdue University, West Lafayette, Indiana, USA*
[106]*Research Division and ExtreMe Matter Institute EMMI, GSI Helmholtzzentrum für Schwerionenforschung GmbH, Darmstadt, Germany*
[107]*Rudjer Bošković Institute, Zagreb, Croatia*
[108]*Russian Federal Nuclear Center (VNIIEF), Sarov, Russia*
[109]*Saha Institute of Nuclear Physics, Kolkata, India*
[110]*School of Physics and Astronomy, University of Birmingham, Birmingham, United Kingdom*
[111]*Sección Física, Departamento de Ciencias, Pontificia Universidad Católica del Perú, Lima, Peru*
[112]*SSC IHEP of NRC Kurchatov institute, Protvino, Russia*
[113]*Stefan Meyer Institut für Subatomare Physik (SMI), Vienna, Austria*
[114]*SUBATECH, IMT Atlantique, Université de Nantes, CNRS-IN2P3, Nantes, France*
[115]*Suranaree University of Technology, Nakhon Ratchasima, Thailand*
[116]*Technical University of Košice, Košice, Slovakia*
[117]*Technical University of Split FESB, Split, Croatia*
[118]*The Henryk Niewodniczanski Institute of Nuclear Physics, Polish Academy of Sciences, Cracow, Poland*
[119]*The University of Texas at Austin, Physics Department, Austin, Texas, USA*
[120]*Universidad Autónoma de Sinaloa, Culiacán, Mexico*
[121]*Universidade de São Paulo (USP), São Paulo, Brazil*
[122]*Universidade Estadual de Campinas (UNICAMP), Campinas, Brazil*
[123]*Universidade Federal do ABC, Santo Andre, Brazil*
[124]*University of Houston, Houston, Texas, USA*
[125]*University of Jyväskylä, Jyväskylä, Finland*
[126]*University of Liverpool, Liverpool, United Kingdom*
[127]*University of Tennessee, Knoxville, Tennessee, USA*

[128] *University of the Witwatersrand, Johannesburg, South Africa*
[129] *University of Tokyo, Tokyo, Japan*
[130] *University of Tsukuba, Tsukuba, Japan*
[131] *Université Clermont Auvergne, CNRS/IN2P3, LPC, Clermont-Ferrand, France*
[132] *Université de Lyon, Université Lyon 1, CNRS/IN2P3, IPN-Lyon, Villeurbanne, Lyon, France*
[133] *Université de Strasbourg, CNRS, IPHC UMR 7178, F-67000 Strasbourg, France, Strasbourg, France*
[134] *Università degli Studi di Pavia, Pavia, Italy*
[135] *Università di Brescia, Brescia, Italy*
[136] *V. Fock Institute for Physics, St. Petersburg State University, St. Petersburg, Russia*
[137] *Variable Energy Cyclotron Centre, Kolkata, India*
[138] *Warsaw University of Technology, Warsaw, Poland*
[139] *Wayne State University, Detroit, Michigan, USA*
[140] *Wigner Research Centre for Physics, Hungarian Academy of Sciences, Budapest, Hungary*
[141] *Yale University, New Haven, Connecticut, USA*
[142] *Yonsei University, Seoul, Republic of Korea*
[143] *Zentrum für Technologietransfer und Telekommunikation (ZTT), Fachhochschule Worms, Worms, Germany*

[*] Dipartimento DET del Politecnico di Torino, Turin, Italy.
[†] Georgia State University, Atlanta, Georgia, USA.
[‡] M. V. Lomonosov Moscow State University, D. V. Skobeltsyn Institute of Nuclear, Physics, Moscow, Russia.
[§] Department of Applied Physics, Aligarh Muslim University, Aligarh, India.
[‖] Deceased.
[¶] Institute of Theoretical Physics, University of Wroclaw, Poland.